Marine Geology 423 (2020) 106134

Contents lists available at ScienceDirect

Marine Geology

journal homepage: www.elsevier.com/locate/margo

Numerical simulation of mid-Holocene tidal regime and storm-tide inundation in the south Yangtze coastal plain, East China

Shuo Wang[a,b,c], Jianzhong Ge[a], K. Halimeda Kilbourne[d], Zhanghua Wang[a,b,e,*]

[a] State Key Laboratory of Estuarine and Coastal Research, East China Normal University, Shanghai 200241, China
[b] Institute of Urban development, East China Normal University, Shanghai 200062, China
[c] Department of Natural Sciences, University of Maryland Eastern Shore, Princess Anne, MD 21853, USA
[d] Chesapeake Biological Laboratory, University of Maryland, Box 38, Solomons, MD 20688, USA
[e] Southern Marine Science and Engineering Guangdong Laboratory (Zhuhai), Zhuhai 519080, China

ARTICLE INFO

Editor: Shu Gao

Keywords:
Coastal flooding
Paleo-topographic change
Tidal amplification
Sea-level rise
Neolithic Liangzhu Culture

ABSTRACT

Coastal flooding is reported as one of the major causes for the interruptions of Neolithic cultures inhabiting the south Yangtze coastal plain, China during the middle Holocene. The archaeologically sterile transgressive sedimentary layers could be the results of extreme events or relative sea-level rise induced by the enlargement of the local tidal range or global/regional sea-level rise. To clarify the mechanism of the transgressive deposits at typical Neolithic sites and the termination of Neolithic Liangzhu Culture in the south Yangtze coastal plain, this study reconstructed the paleo-topography at 7.6, 6.4 and 4.5 cal ka BP on the basis of a database including 107 sediment cores and 644 radiocarbon ages and simulated the paleo-tidal regimes and the inundation areas induced by typhoon events under the paleo-topography and sea levels using a hydrodynamic model of high-resolution Changjiang Estuary Finite-Volume Community Ocean Model (CE-FVCOM). The simulation results of tidal regimes showed that the tidal amplitude increased from 1.6 m to 2.2 m in the head of Hangzhou Bay induced by the paleo-topographic change during the period 7.6–4.5 cal ka BP. By contrast, it reduced from 1.6 m to 1.0–1.2 m in the Ningbo Plain, southeast of the bay, which was unable to explain the long-lasting marine inundation there and supported our previous assumption of an event of abrupt sea-level rise at 4.5–4.4 cal ka BP. Simulation of the storm-induced inundation further suggested that coastal flooding mainly occurred along the coastline of the Taihu Plain under the combined effect of tidal amplification and typhoon events at 4.5 cal ka BP, while the inundation almost covered half of the Taihu Plain if all factors including tidal amplification, extreme event and the abrupt sea-level rise were considered. We therefore suggest that the obvious increase in flood risk under the backdrop of sea-level rise was a major cause for the abandonment of the Liangzhu Culture in the south Yangtze coastal plain at around 4.4 cal ka BP.

1. Introduction

Coastal flooding from extreme water levels is considered as a major risk for coastal low-lying areas worldwide (Grinsted et al., 2013; Woodruff et al., 2013; Hinkel et al., 2014; Long et al., 2014, Neumann et al., 2015) because global sea-levels were predicted to rise between 0.2 and 2.4 m by the end of the 21st century depending on future greenhouse forcing (Rogelj et al., 2012; Wong et al., 2017; Nauels et al., 2017; Kopp et al., 2017; Jackson et al., 2018). In addition, global warming will enhance the ocean-atmosphere coupling, leading to an increase in the number of 'strong' El Niño and associated extreme weather events (Zhang et al., 2012; Cai et al., 2018). In the densely-populated Yangtze (Changjiang) Delta, East China, flood risk from extreme events and sea-level rise was estimated to increase by 150% to 400% over the next 50 years from an analysis by Tessler et al. (2015).

Neolithic cultures on the low-lying south Yangtze coastal plain around Hangzhou Bay (Fig. 1) had also been vulnerable to the coastal flooding in the middle Holocene. Previous studies reported layers of natural deposits (i.e. "artefacts-absent layers") frequently found covering the prehistoric cultural layers of the Kuahuqiao, Hemudu and Liangzhu Cultures on the south bank of Hangzhou Bay, and they were often composed of sediments of marine origin (Zong et al., 2007; Zheng et al., 2009; He et al., 2018; Wang et al., 2018a). Recent work further revealed evidences of flooding across the south Yangtze coast at the terminal stage of the Liangzhu Culture (Zong et al., 2011, 2012) and proposed an event of abrupt sea-level rise after ca. 4.5 cal ka BP linked

* Corresponding author at: State Key Laboratory of Estuarine and Coastal Research, East China Normal University, Shanghai 200241, China.
E-mail address: zhwang@geo.ecnu.edu.cn (Z. Wang).

https://doi.org/10.1016/j.margeo.2020.106134
Received 6 June 2019; Received in revised form 23 December 2019; Accepted 13 January 2020
Available online 30 January 2020
0025-3227/ © 2020 Elsevier B.V. All rights reserved.

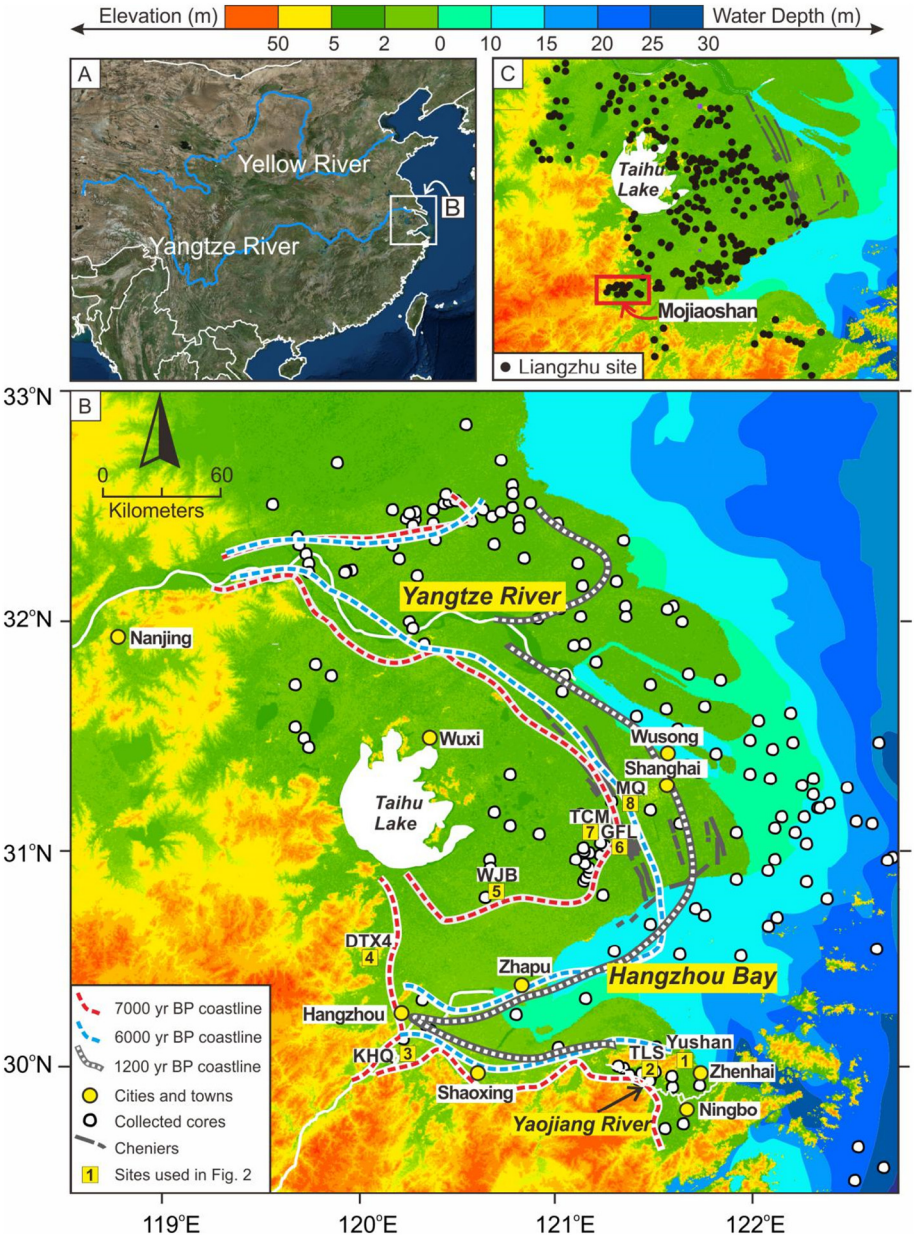

Fig. 1. Location maps. (A) East Asia and the location of the study area. (B) The Yangtze Delta plain on the north bank and the Ningbo-Shaoxing coastal plain on the south bank of Hangzhou Bay, showing the location of sediment cores we have compiled from previous publications. The paleo-coastlines were after Zhang et al. (2015) and bathymetry was after Ge et al. (2013). (C) The southern Yangtze Delta plain, showing the locations of the Neolithic Liangzhu sites and Liangzhu's capital city Mojiaoshan. The maps were generated with the ArcGIS 10.1 software (www.esrichina.com.cn) using the topographic dataset provided by the International Scientific & Technical Data Mirror Site, Computer Network Information Centre, Chinese Academy of Sciences (http://www.gscloud.cn).

to the decline of the Culture (Wang et al., 2018a).

However, the formation mechanism of these transgressive deposits is still debated. First, the south Yangtze coastal plain lies close to the usual tracks of tropical cyclones that approach land along the west coast of the Northwest Pacific basin (Woodruff et al., 2013). According to Chinese historical literature, there have been 201 severe storm surges on the Yangtze coast over past 2000 years (Xu, 1997). Thus the marine deposits covering the Neolithic cultural layers could be storm overwash during the extreme typhoon events. We did not consider winter storms because the wind direction of winter storm is generally toward offshore region and thus has limited impact on the coastal morphology (Xu, 1997). We neither consider the tsunamis because the wide shallow continental shelf of the East China Sea protects the Yangtze coast from tsunami events by having the potential to dissipate the energy of large waves (Ren et al., 2013).

Second, the rise in peak sea level could also be a result of an increase in the local tidal range, owing to the changes in paleo-topography, which is an important factor in controlling tidal regimes in coastal areas (Winterwerp et al., 2013). Tidal amplification was reported in the paleo-Yangtze Estuary in the middle Holocene by numerical simulation (Uehara et al., 2002; Uehara and Saito, 2003). We propose it could also have occurred in Hangzhou Bay as there were obvious changes in the coastlines, and the shape converged to the head of the bay in the middle Holocene (Fig. 1B; Zhang et al., 2015a). Therefore, the previously reconstructed relative sea levels for the south Yangtze coastal plain (Wang et al., 2012, 2013, 2018a) could be overestimated since they did not consider the potential enlargement of the tidal range. We suggest that it is necessary to examine the spatial and temporal changes in tidal levels along with the changes in paleo-topography to better understand the relative sea-level changes in the middle Holocene.

Overall, the transgressive sediments covering cultural layers could be the results of extreme events or relative sea-level rise induced by the enlargement of the regional tidal range or global/regional sea-level rise. To clarify these three factors, in this study we collected all published sediment cores and sediment profiles at Neolithic sites from Hangzhou Bay and its southern coastal plain. Together with the sediment cores/profiles compiled in Wang et al. (2018b) and Chen et al. (2018), we identified 107 high-quality sediment cores/profiles and 644 absolute ages (supplementary Tables S1, S2), and used them to reconstruct the paleo-topography at 7.6, 6.4 and 4.5 cal ka BP, which are roughly the

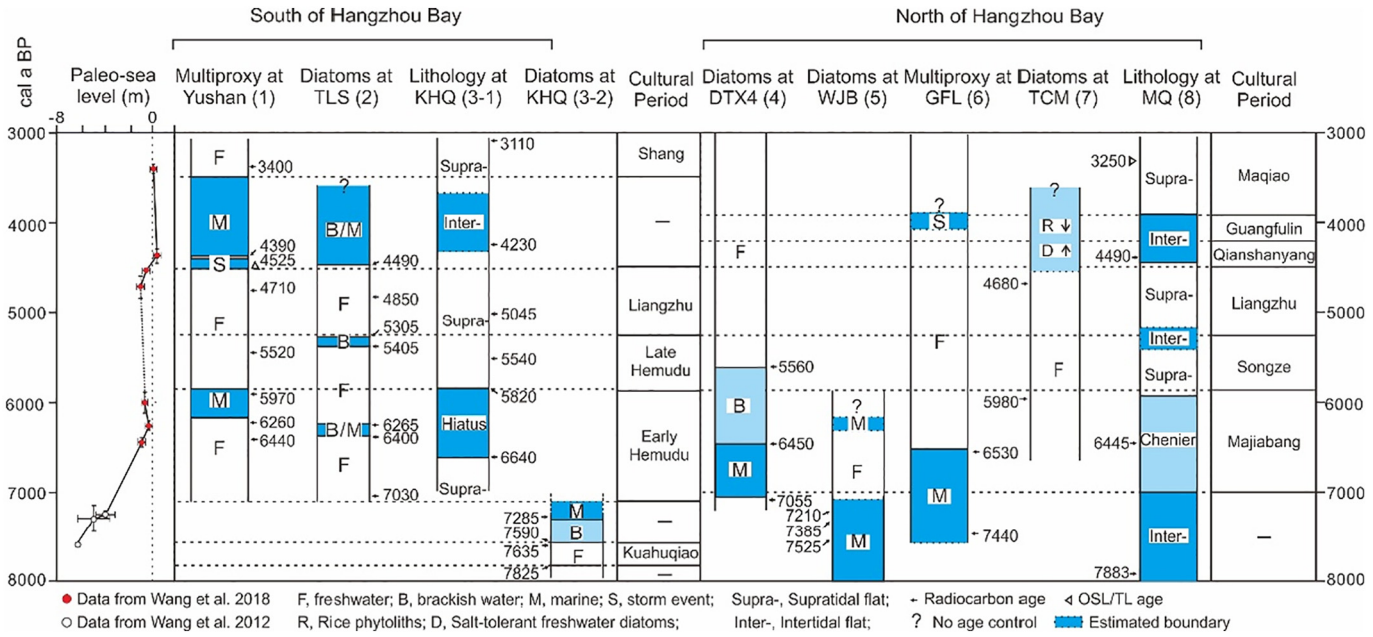

Fig. 2. Comparison of the relative sea-level curve (Wang et al., 2012, 2018a) and regional marine inundation records on the south and north banks of Hangzhou Bay. In sea-level curve, calibrated radiocarbon ages are presented with error bars of 2σ; horizontal error bars represent the indicative meaning (range of relative sea level) of each sea-level indicator. Locations of sediment profiles are shown in Fig. 1. Sea-level data are given in Supplementary Table S3.

beginning ages of transgression events in the Neolithic period in the study area (Fig. 2). We then simulated the paleo-tidal regimes and inundation areas induced by storm-tides changing with the paleo-topography at the three stages using a hydrodynamic model of high-resolution Finite-Volume Community Ocean Model (FVCOM; Chen et al., 2003). We suggest that our simulation will help constrain the amplitude of abrupt sea-level rise after 4.5 cal ka BP and clarify the vulnerability of the coastal Neolithic societies to the extreme events and relative sea-level rise.

2. The study area, Neolithic cultures and mid-Holocene coastal flooding

The south Yangtze coastal plain is divided by Hangzhou Bay into a north and a south part, i.e. the southern Yangtze Delta Plain including the Taihu Plain on the north bank, and the Shaoxing and Ningbo Plains on the south bank of the bay (Fig. 1B). Hangzhou Bay, ca. 100 km long, is a funnel-shaped and shallow estuary, covering an area of approximately 8500 km^2. It is ca. 100 km wide at the mouth and narrows sharply landward to ca. 25 km wide at Zhapu, ca. 100 km inland from the mouth (Fig. 1B). The average water depth in the bay is 8–10 m during low tides (Xie et al., 2009). Main river systems discharging into Hangzhou Bay, i.e., the Qiantang and Cao-e Rivers have a total runoff of only ca. 42 $km^3\ yr^{-1}$ and a total sediment load of ca. 7.9×10^6 t yr^{-1} (ECCHE, 1992; Milliman and Syvitski, 1992). Diluted water and suspended sediments from the Yangtze River mouth play an important role in the infilling of Hangzhou Bay both during the Holocene and at present day (Milliman et al., 1985; Gao and Collins, 2014). Semi-diurnal tides occur in Hangzhou Bay, with the M_2 constituent being the dominant tidal component (ECCHE, 1992). The tidal range is 3–4 m at mouth and 4–6 m further upstream, and the maximal flood velocity exceeds 3.0 m/s (Xie et al., 2009; ECCHE, 1992). By contrast, the tidal range is only 1.85 m, recorded at Zhenhai tidal gauge station (Fig. 1B) on the coast of Ningbo Plain, southeast of Hangzhou Bay. In addition, ground altitude in most parts of the Taihu and Ningbo Plains is 0–2 m, while the ground altitude of the peripheral region, i.e. the plain along the shoreline of the bay is 2–5 m. Typhoon activities around Hangzhou Bay are most frequent in July to September. For example, on August 1, 1956, Typhoon Wanda caused a storm surge of 4.57 m at Zhapu station and widespread flooding in adjacent low-lying areas on the north bank of the bay (Zheng and Yu, 2013).

Neolithic settlings appeared in the south Yangtze coastal plain soon after the initiation of the Delta at around 8000 cal a BP because the rate of sea-level rise at that time greatly reduced compared with the early Holocene (Hori et al., 2001; Wang et al., 2013). Two systems of Neolithic cultures have been recognized on the south and north banks of Hangzhou Bay, respectively (Fig. 2). The major Neolithic culture phases include the Kuahuqiao (7800–7600 cal a BP; Zong et al., 2007; Innes et al., 2009), early Hemudu (7200–5800 cal a BP), late Hemudu (5700–5300 cal a BP), and Liangzhu (5300–4400 cal a BP; Li et al., 2010) Cultures in the coastal plain on the south bank. On the north bank, the settling started as the Majiabang Culture (7000–5800 cal a BP), followed by Songze (5800–5300 cal a BP), Liangzhu (5300–4400 cal a BP), Qianshanyang (4400–4200 cal a BP), and Guangfulin Cultures (4200–3900 cal a BP; Chen et al., 2007; Long et al., 2014; Wang et al., 2018a). In particular, the Liangzhu Culture had entered a civilized society of initial state scale, with its developed rice farming, a large number of exquisite jades and potteries, as well as the social stratification reflected by graves and large-scale civil engineering projects (Li et al., 2010; Liu et al., 2017). The settlements of Liangzhu Culture are mainly distributed in the lowland around the Taihu Lake and Hangzhou Bay, whereas the coastal plain on south bank of the bay is considered to be the extension area (Li et al., 2010; Fig. 1C). After the sudden interruption of the Liangzhu Culture at about 4500 years ago, the subsequent Neolithic cultures, particularly the Guangfulin Culture, were considered to be mainly migrated from northern China (Song et al., 2002).

Many studies have reported sedimentary records of both marine and inland flooding at Neolithic sites in the south Yangtze coastal plain during the mid-Holocene (Fig. 2; Zong et al., 2007; Qin et al., 2011; Zong et al., 2011; Zheng et al., 2012; Chen et al., 2018; Wang et al., 2018a; Tang et al., 2019). Marine and brackish water diatoms, intertidal fungal spores and marine dinoflagellate cysts in the deposits overlying the Kuahuqiao cultural layer at the Kuahuqiao (KHQ) site at the head of Hangzhou Bay reflected an event of marine inundation at 7550 cal a BP, which resulted in the termination of dwelling and

cultivation at the site (Zong et al., 2007; Innes et al., 2009). At Neolithic Tianluoshan (TLS) and Yushan sites in the southeast coastal plain of Hangzhou Bay, sedimentary records indicated at least two transgressive layers dated at ca. 6400–6300 cal a BP and ca. 4500 cal a BP, respectively (Zheng et al., 2012; He et al., 2018; Wang et al., 2018a). On the north bank of Hangzhou Bay, there is widespread evidence of marine transgression at ca. 6500 cal a BP (Fig. 2; Qin et al., 2011; Wang et al., 2012; Chen et al., 2018). Subsequently, marine inundation was mainly found at sites close to the shoreline. For example, at the Maqiao site on the chenier ridge, it was a supratidal environment before the settling of Liangzhu people and flooding occurred at ca. 4490 cal a BP, as evidenced by an artefacts-absent layer of sediments between the Liangzhu and Maqiao cultural layers (Yu et al., 1998; Cheng and Song, 1999). By contrast, in the inland plain protected by the chenier ridges, marine influence was weak but a rise of local water level was reported for many sites at the terminal stage of Liangzhu Culture (Zong et al., 2011, 2012; Tang et al., 2019). For example, at the Tangcunmiao (TCM) site, there was an increase in the brackish water-tolerant diatom species and a reduction in rice phytoliths after ca. 4680 cal a BP (Zong et al., 2011). At the GFL site, the sedimentary records of pollen indicated an expansion of marsh at ca. 4500 cal a BP (Tang et al., 2019). In addition, deposits of storm events between ca. 4500–4200 cal a BP have been recovered at Yushan and GFL sites on both north and south banks of Hangzhou Bay (Wang et al., 2018a; Tang et al., 2019). Thus, there were three major stages of coastal flooding starting at ca. 7.6, 6.4 and 4.5 cal ka BP, respectively in the south Yangtze coastal plain (Fig. 2).

3. Methods

3.1. Reconstruction of the paleo-topography

Our previous studies have compiled > 300 sediment cores and profiles and 658 radiocarbon ages from the area of Yangtze coast and adjacent continental shelf (Chen et al., 2018; Wang et al., 2018a, 2018b). In this study, we further collected 37 sediment cores and profiles with 87 radiocarbon ages from previous publications from Hangzhou Bay and its coastal plain. We then identified 107 sediment cores and profiles (Table S1) as having robust chronological controls (644 radiocarbon ages in total; Table S2) for the Holocene period, based on an examination of the database of each core and profile including location, dating depth, dating results and references. All radiocarbon ages were calibrated using software Calib 7.1 (Stuiver et al., 2018). The Marine 13 calibration curve was used for marine mollusk shell samples and a ΔR value of 135 ± 42 was used to correct for the marine reservoir effect (Yoneda et al., 2007). Age-depth models for each sediment core or profile were constructed, taking into account the probability distribution of each calibrated age, with the program 'Clam' using linear interpolation and 10,000 iterations (Blaauw, 2010). The buried depth (calibrated to the present mean sea level) at 7.6, 6.4 and 4.5 cal ka BP at each core site was thus calculated (Table S1) according to the age-depth model, and this database was used to reconstruct the paleo-topography of the south Yangtze coast at 7.6, 6.4 and 4.5 cal ka BP (Fig. 3). Land subsidence should be considered as a factor when reconstructing the paleo-topography. However, GPS monitoring demonstrated negligible land subsidence at our core locations during the last half-century (Zhang et al., 2008). Simulation by Song et al. (2013) demonstrated that the glacio-hydro-isostatic effect on the vertical land movement on the southern Yangtze Delta Plain was < 0.1 m for the present cores. Therefore, local factors controlling vertical land movement may be neglected for the paleo-topography in the Neolithic period explored in this study. Thus, the paleo-topography at each stage was calibrated by comparing the burial depths with the paleo-sea levels at 7.6, 6.4 and 4.5 cal ka BP, which was ca. −6.3 m, −1.5 m and −0.7 m, respectively (Wang et al., 2012, 2018a).

3.2. Numerical model and experiments

In this work, the high-resolution, unstructured-grid-based, 3D modeling system FVCOM (Finite-Volume Community Ocean Model; Chen et al., 2003) was applied to estimate the paleo-tidal regime and storm-induced inundation at 7.6, 6.4, 4.5 cal ka BP in the south Yangtze coastal plain, East China. This model has proven to be an excellent tool to simulate the coastal inundation under storm impact (Zhao et al., 2014). A similar model system based on FVCOM was also established for the East China Sea and Changjiang (Yangtze) Estuary (ECS-CE) (Ge et al., 2013). This model system has been validated using various observational data, including surface wind, tides, currents, salinity, and waves to accurately reveal the multi-scale dynamics, particularly for the tide propagation around the East China Sea and Changjiang (Yangtze) Estuary (Ge et al., 2013). The unstructured mesh provides accurate fitting along the irregular geometric boundaries, such as coastlines and islands (Fig. 4).

To resolve the highly variable bathymetry and complex geometry of marginal seas, coasts, islands and tidal channels, unstructured grids (51,480 nodes and 95,423 elements) with variable sizes and orientations were used in the numerical model (Fig. 4A–C). The mesh domain covered the marginal seas including the Bohai Sea, Yellow Sea, East China Sea, and Japan Sea and part of the west Pacific Ocean with a resolution of 25 km (Fig. 4A); the grid resolution increased gradually to 1 km at the boundaries of the Yangtze Estuary and Hangzhou Bay (Fig. 4B) and grid sizes were < 0.5 km in the shallow regions of the Ningbo Plain (Fig. 4C).

The model was forced by sea surface wind and tide constituents. Eight major astronomical tide constituents, M_2, S_2, K_2, N_2, K_1, O_1, P_1 and Q_1, were added along the open boundary, obtained from Global Inverse Tidal Model TPXO 8.0 (Egbert and Erofeeva, 2002), and were adopted to determine the water elevation. The water column has been numerically discretized into ten uniform sigma layers. In this study, only typhoon wind was considered to determine its impact on the coastal flooding around the south Yangtze coastal plain. The symmetry of the typhoon model was calculated using the Fujita formula to determine the pressure gradient-induced cyclonic wind (Fujita, 1952). Additionally, the wind component from the typhoon's movement was estimated by the Miyazaki formula (Miyazaki et al., 1961).

For the bathymetry settings, the paleo-bathymetry reconstructed from sediment cores was used in the model along the Yangtze Estuary and Hangzhou Bay (the region between latitude 29–33°N and longitude 119–123.5°E; Fig. 3), where the paleo-topography has been greatly changed by sea-level rise and deposition/erosion during the Holocene (Fig. 3; Wang et al., 2018b). For other regions with little Holocene sedimentation, the present bathymetry was used to be calibrated into the paleo-bathymetry by comparison with the paleo-sea levels.

In order to simulate accurately over realistic bathymetric inter-tidal zones (i.e., the grid that experiences both flooding and drying in the model) over tidal cycles and storm events, the wet/dry point treatment method in the FVCOM was applied, which has been validated in a series of tidal simulations in an idealized semi-enclosed estuary with an inter-tidal zone (Chen et al., 2003). Defining the local summation of water depth $D = H_m + \zeta$, where $H_m = H + D_{min}$ in the water and $H_m = -(h_B + D_{min})$ on the land; H is the reference water depth, ζ is the surface elevation and h_B is the land height. For the wet or dry criterion for node points, the criterion is given as

$$\begin{cases} wet,\ if\ D = H_m + \zeta > D_{\min} \\ dry,\ if\ D = H_m + \zeta \le D_{\min} \end{cases}$$

and for triangular cells is given as

$$\begin{cases} wet,\ if\ D = \min(H_{m,i}, H_{m,j}, H_{m,k}) + \max(\zeta_i, \zeta_j, \zeta_k) > D_{\min} \\ dry,\ if\ D = \min(H_{m,i}, H_{m,j}, H_{m,k}) + \max(\zeta_i, \zeta_j, \zeta_k) \le D_{\min} \end{cases}$$

where D_{min} is the thickness of the viscous layer specified at the bottom,

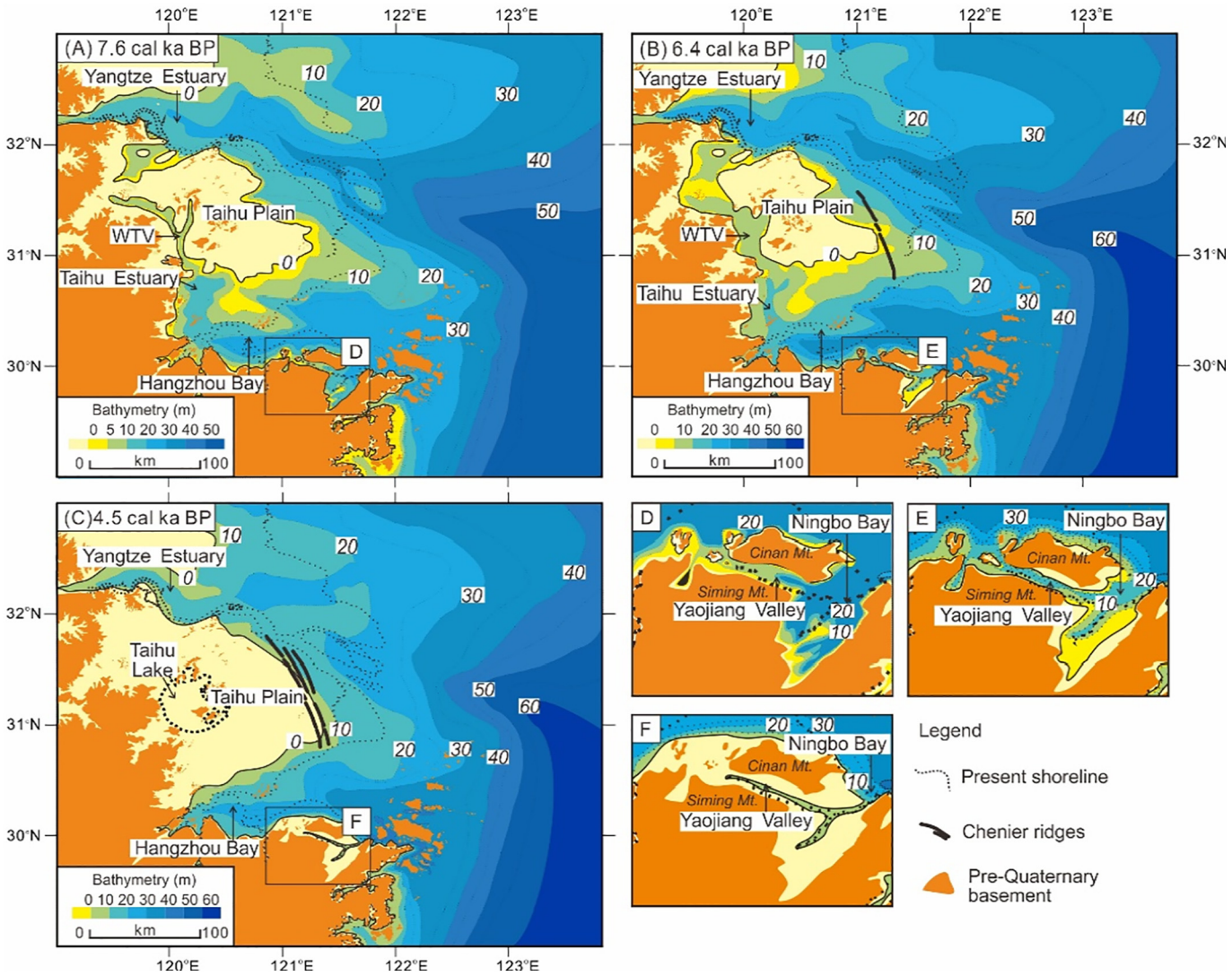

Fig. 3. Paleo-topographic map of the southern Yangtze Delta plain and the south bank of Hangzhou Bay at (A) 7.6 cal ka BP, (B) 6.4 cal ka BP, and (C) 4.5 cal ka BP. Abbreviation: WTV, west Taihu Valley. (D), (E), (F) shows the paleo-topography in the Yaojiang Valley and Ningbo Plain at 7.6, 6.4 and 4.5 cal ka BP. Locations of the sediment cores for paleo-topographic reconstruction are shown in Fig. 1B. Details including dating depth, dating results and references of each sediment core are provided in Supplementary Table S2.

and i, j, k are the integer numbers to identify the three node points of a triangular cell. Cells which were dry at the time of mean spring low water (MSLW) and wet at the time of mean spring high water (MSHW) in the simulation results were defined as the intertidal zone. We further defined the wet cells exceeding the simulated landward boundary of intertidal zone at the time of highest water levels (HWL) in typhoon scenarios as the flooding area induced by storms.

According to the meteorological records over past decades, the typhoons which obviously impacted the south Yangtze coast most frequently landed at a distance of ca. 250 km south to Hangzhou Bay and moved northward and northwestward (Ying et al., 2014). Typhoon Winnie (TP9711) landing on August 18, 1997 and Typhoon Matsa (TP0509) landing on August 6, 2005 (Table 1; tcdata.typhoon.org.cn) were two representative storms among those having caused obvious storm surges and wide inundations in the south Yangtze coastal plain over past decades (Wang et al., 2010). This study thus used these two strong but distinct storms as the typhoon scenarios to simulate the storm-induced inundation in the middle Holocene.

Typhoon 9711 was one of the strongest storms among the 313 typhoon events landing the east and southeast China coast over past 60 years (Ying et al., 2014). It landed on Wenling, 233 km away from Hangzhou Bay with a central pressure of 960 hPa, wind velocity of 40 m/s and radius of strong gale of 600 km, and moved northwestward (Fig. 5A; tcdata.typhoon.org.cn). The lowest central pressure of Typhoon 9711 reached 920 hPa and maximum wind speed was 60 m/s before its landing. It induced a peak tidal elevation as high as 4.32 m (Yellow Sea datum) at the Wusong station of Yangtze River mouth (Xu et al., 2007). Storm surge during the landing was significant with an increase in water level of ca. 0.8 m at more than half of tidal gauge stations along the coastlines of Hangzhou Bay and Yangtze River mouth (Fig. 5B; Ye, 1999; Ge, 2007). Typhoon 0509 landed on Yuhuan, 260 km away from Hangzhou Bay with a central pressure of 950 hPa, wind velocity of 45 m/s and radius of strong gale of 500 km, and moved northward to northwestward thereafter (Fig. 5A). The lowest central pressure of this typhoon was 950 hPa and maximum wind speed was 45 m/s (Table 1). It induced a highest tidal level of 3.37 m (Yellow Sea datum) at the Wusong station (Xu et al., 2007) and an increase in water level of ca. 0.4–0.6 m along the coastlines of Hangzhou Bay and Yangtze River mouth during its landing (Fig. 5B; Ge, 2007).

In total, 12 experiments were conducted under different historical conditions and typhoon scenarios (Table 2). Each experiment consisted of a one-month-long simulation with 0.5 s time steps. In order to obtain

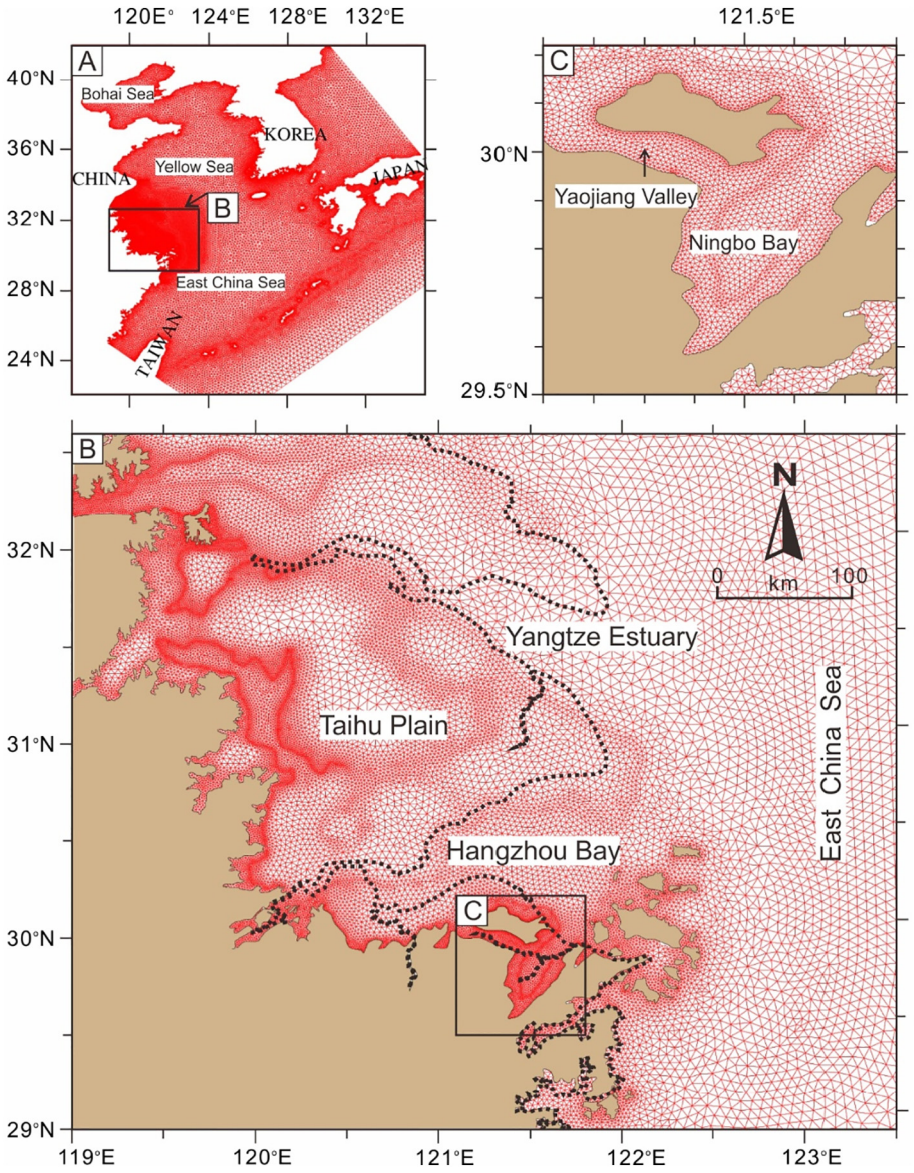

Fig. 4. High-resolution triangle grids for the (A) East China Sea and its adjacent regions with resolutions of 25 km; (B) Yangtze Estuary, Hangzhou Bay and its adjacent regions with resolutions of 1–5 km; (C) region of Yaojiang Valley and Ningbo Bay with resolutions of 0.5 km.

the mid-Holocene tidal regimes, the base cases (Table 2: Case 1 to Case 3) were simulated only under the influence of astronomical tides without typhoon occurrence, using the bathymetric data at 7.6, 6.4, and 4.5 cal ka BP, respectively. The spatial and temporal distributions of mean spring high water (MSHW), which was represented by the highest tide level in this one-month-long simulation, were presented in Table 3 and Figs. 6A–C, 7. The Cases 4, 5 and 6 were configured to consider the impact of Typhoon 0509 with different historical bathymetries; similarly, Case 7–9 simulated Typhoon 9711.

To obtain the maximum inundation area of storm, the typhoon landing time was set to match the moment of the monthly highest astronomical tide level in the modeling. The distribution of highest water levels (HWL) in the simulations of two typhoon scenarios were presented in Table 3 and Figs. 6 D–I, 7. Furthermore, a scenario of relative sea-level rise (SLR) for 0.95 m from 4.5 to 4.4 cal ka BP (Wang et al., 2018a) was adopted for the simulation of astronomic and storm tides at 4.4 cal ka BP (Table 2: Case 10 to Case 12). The bathymetry at 4.4 cal ka BP was taken from the bathymetry at 4.5 cal ka BP adding the SLR due to little change in paleo-topography within the 100 years.

4. Results

4.1. The mid-Holocene basin geometry of the south Yangtze coast

Our reconstruction of the paleo-bathymetry and paleo-coastline (water depth line of 0 m, Fig. 3) documented changes in the basin geometry at the south Yangtze coast during the period between 7.6 and 4.5 cal ka BP. We identified six sub-basins according to the paleo-topography, which consisted of the Yangtze Estuary, Hangzhou Bay, west Taihu Valley (WTV), paleo-Taihu Estuary, Ningbo Bay, and Yaojiang Valley (Fig. 3).

Under the background of rapid sea-level rise (Wang et al., 2012), the paleo-Yangtze River mouth, Hangzhou Bay, and Taihu Estuary were all inundated by seawater at 7.6 cal ka BP and a water depth of about 20–25 m occurred in the paleo-Hangzhou Bay, more than twice as deep as it is today (Fig. 3A). The Taihu Plain was surrounded by the seawater at the east, south and west sides. On the south coast of Hangzhou Bay, the water depth in Ningbo Bay was mostly shallower than 25 m, while the water depth in the Yaojiang Valley was mostly between 5 and 15 m, due to the protection by the Cinan and Siming Mountains (Fig. 3D).

Table 1
The intensity comparison between Typhoon 9711 and Typhoon 0509. Dataset is obtained from tcdata.typhoon.org.cn .

		Date	Center location	Central pressure (hPa)	Maximum wind speed (m/s)	Distance from Hangzhou Bay (km)	Radius of strong gale (Force 7 wind)[a] (km)	Radius of storm (Force 10 wind)[a] (km)
Typhoon 9711	Landfall	1997-08-18 20:00:00	Wenling, China	960	40	233	600	200
	Maximum intensity	1997-08-12 20:00:00	18.1°N, 144.8°E	920	60	2677	–	–
Typhoon 0509	Landfall	2005-08-06 02:00:00	Yuhuan, China	950	45	260	500	180
	Maximum intensity	2005-08-04 20:00:00	24.6°N, 124.3°E	950	45	795	600	200

[a] Based on the Beaufort wind force scale.

At 6.4 cal ka BP, the largest transgression area in the Holocene occurred in the south Yangtze Delta plain (Fig. 3B; Hong, 1991; Chen et al., 2018). The paleo-Taihu Estuary was possibly connected to the Yangtze Estuary through the west Taihu Valley, making the Taihu Plain isolated as an island (Fig. 3B). The Yaojiang Valley was completely flooded by seawater, connecting Ningbo Bay to the east and Hangzhou Bay to the west (Fig. 3E). The southern coastline of Hangzhou Bay was located on the north edge of the Siming Mountain at that time. However, due to the deceleration of sea-level rise between 7.2 and 6.4 cal ka BP (Wang et al., 2012, 2018a), rapid sedimentation occurred in the Yangtze Estuary, paleo-Taihu Estuary and Hangzhou Bay, which resulted in a shallowing in these areas although the coastlines retreated landward significantly in the south Yangtze Delta plain. On the south coast of Hangzhou Bay, deposition also occurred in Ningbo Bay and along the foothills of the Cinan Mountain. The coastline of Ningbo Bay even advanced seawards, possibly due to the shadowing effect for transgression of the Cinan Mountain (Fig. 5E).

At 4.5 cal ka BP, the west Taihu Valley and paleo-Taihu Estuary were infilled and a freshwater environment prevailed there (Fig. 3C; Chen et al., 2018). Hangzhou Bay therefore was separated from the Yangtze Estuary by the Taihu Plain and basically formed its funnel shape (Zhang et al., 2012). Several chenier ridges about 0.5–2 m high developed on the east coast of Taihu Plain, marking the location of the coastline at that time (Liu and Walker, 1989). On the south bank of Hangzhou Bay, Ningbo Bay and Yaojiang Valley were mostly infilled, connected to Hangzhou Bay mainly by tidal rivers (Fig. 3F). As a result, the south coastline of Hangzhou Bay advanced to the north edge of the Cinan Mountain.

4.2. Simulation of the paleo-tides

Simulation results demonstrated that after the tides from the Pacific Ocean propagated into the East China Sea (ECS), part of the tidal wave further propagated northwest to the Yellow Sea, while others reached the Yangtze coast and spread into Hangzhou Bay. An overall increase in the tidal range northward and landward occurred in the coastal region of the ECS at the three stages. Such tidal amplification was clearer in the sub-basins at the Yangtze coast, with tidal levels generally higher at the head than at the mouth in an estuary or a bay (Fig. 6A–C; Table 3).

The temporal changes of tidal levels during 7.6–4.5 cal ka BP were different in the six sub-basins (Table 3; Fig. 7). Tidal amplification through time was obvious in the paleo-Yangtze Estuary and Hangzhou Bay, particularly in the head of Hangzhou Bay, as reflected by the mean spring high water (MSHW), which increased from 1.6 m to 2.2 m from 6.4 to 4.5 cal ka BP. The increases in MSHW were much weaker from 7.6 to 6.4 cal ka BP. Slight tidal amplification also occurred in the paleo-Taihu Estuary and west Taihu Valley from 7.6 to 6.4 cal ka BP (Fig. 6A, B). By contrast, no tidal amplification occurred from 7.6 to 4.5 cal ka BP on the southeast coast of Hangzhou Bay. Instead, the simulated MSHW declined from 1.4–1.6 m at 7.6 cal ka BP to 1.0–1.4 m at 6.4 cal ka BP and 4.5 cal ka BP in the Yaojiang Valley and Ningbo Bay (Table 3; Fig. 7), despite tidal amplification that occurred in the offshore area from 6.4 to 4.5 cal ka BP (Fig. 6B, C).

The distribution of the intertidal flat from 7.6 to 4.5 cal ka BP was simulated (Fig. 8–10). The spring tides reached the pre-Quaternary bedrock on the south and west coasts of Hangzhou Bay and inundated most part of the west Taihu Valley, paleo-Taihu Estuary, Ningbo Bay and Yaojiang Valley at 7.6 and 6.4 cal ka BP. As a result, the Taihu Plain was surrounded by saltwater on all sides, isolating it from the mainland, and the shape of Hangzhou Bay was a rectangle (Figs. 8, 9). At 4.5 cal ka BP, flooding mainly occurred along the coastal plain of the Yangtze Estuary and the north bank of Hangzhou Bay (Fig. 10). In the Yaojiang Valley and Ningbo Bay which had mostly been infilled, invasion of spring tide only occurred through the tidal river in the coastal plain as protected by pre-Quaternary bedrock along the coast of Hangzhou Bay.

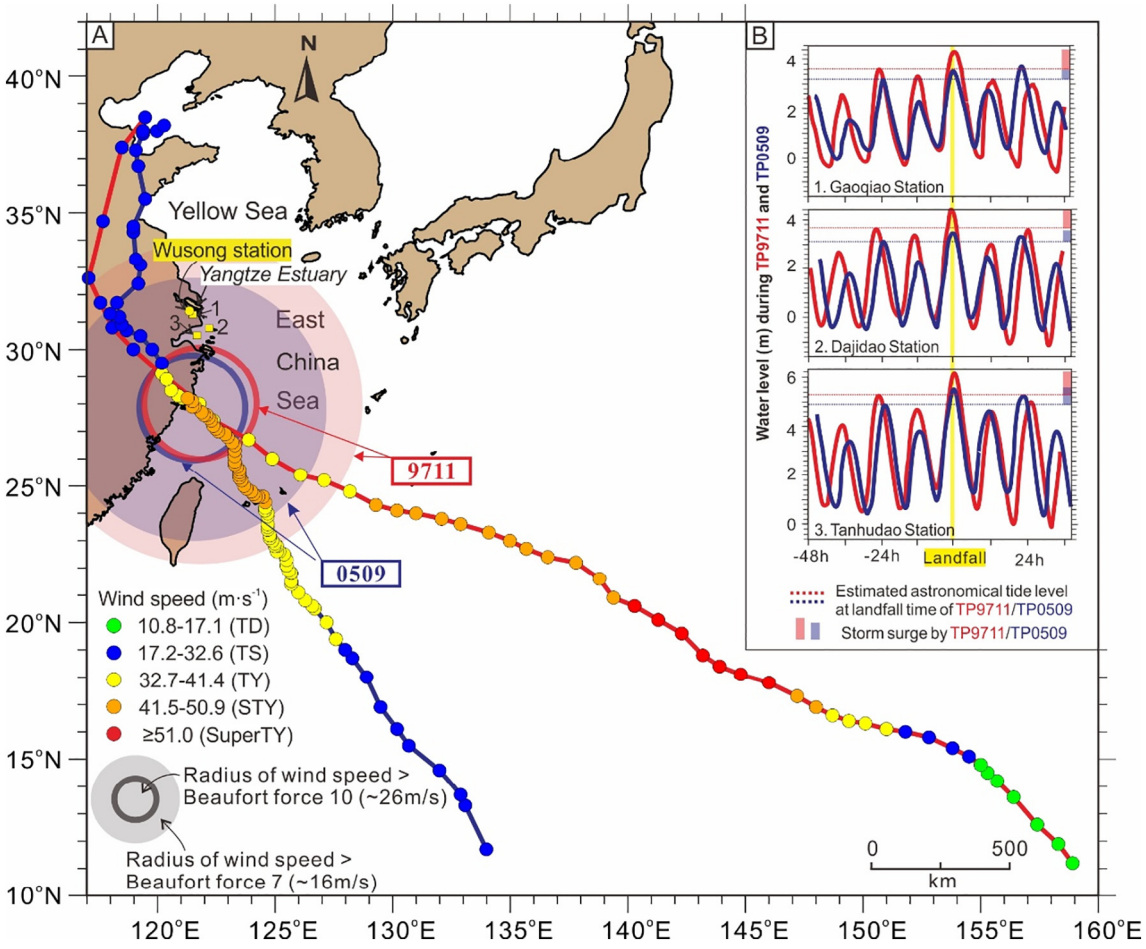

Fig. 5. (A) Observational data of tracks, wind speeds and radii of gale winds at landfall time of Typhoon Winnie (TP9711) and Typhoon Matsa (TP0509) for storm-tide experiments. Intensity category was defined by wind speed: Tropical Depression (TD, 10.8–17.1 m/s), Tropical Storm (TS, 17.2–32.6 m/s), Typhoon (TY, 32.7–41.4 m/s), Severe Typhoon (STY, 41.5–50.9 m/s), and Super Typhoon (SuperTY, ≥51.0 m/s). (B) Curves of observed water levels (Yellow Sea datum) at Gaoqiao, Dajidao, and Tanhudao stations showing the storm surges at the Yangtze coast and Hangzhou Bay during the landing of Typhoon 9711 and Typhoon 0509 (after Ge, 2007). TP9711 in red and TP0509 in blue. (For interpretation of the references to color in this figure legend, the reader is referred to the web version of this article.)

4.3. Storm surge and flooding in the two scenarios of extreme events

Both scenarios of Typhoon 0509 and 9711 caused serious flooding in the south Yangtze Delta plain and coastal plains along Hangzhou Bay in the simulation (Figs. 8–10). The storm surge was much more obvious in Hangzhou Bay, paleo-Taihu Estuary and west Taihu Valley than in the Yangtze Estuary, Yaojiang Valley and Ningbo Bay at all three stages (Table 3; Fig. 7). Particularly at the head of Hangzhou Bay, the highest water level (HWL) of storm surge occurred, which reached 3.2 m at 4.5 cal ka BP in both typhoon scenarios and was 1.0 m higher than the MSHW at that time; the storm surge there was 0.8–1.0 m higher than the MSHW in the two typhoon scenarios at 7.6 and 6.4 cal ka BP. In the paleo-Taihu Estuary, storm surge was also obvious both at its mouth and head, being 0.6–1.2 m higher than the MSHW at 7.6 and 6.4 cal ka BP (Table 3; Fig. 7). By contrast, the storm surge in the two typhoon scenarios was weaker, being 0–0.6 m higher than the MSHW in the

Table 2
Model experiments including the fair weather and two scenarios of typhoon event at 7.6, 6.4 and 4.5 cal ka BP. Three more experiments were made under the sea-level rise scenario at 4.4 cal ka BP.

	Bathymetric data	Typhoon	Start date	End date
Case 1	7.6 cal ka BP	None	2005-07-15 11:00:00	2005-08-15 00:00:00
Case 2	6.4 cal ka BP	None		
Case 3	4.5 cal ka BP	None		
Case 4	7.6 cal ka BP	Typhoon 0509	2005-07-15 11:00:00	2005-08-15 00:00:00
Case 5	6.4 cal ka BP	Typhoon 0509		
Case 6	4.5 cal ka BP	Typhoon 0509		
Case 7	7.6 cal ka BP	Typhoon 9711	1997-07-21 14:00:00	1997-08-21 08:00:00
Case 8	6.4 cal ka BP	Typhoon 9711		
Case 9	4.5 cal ka BP	Typhoon 9711		
Case 10	4.4 cal ka BP	None	2005-07-15 11:00:00	2005-08-15 00:00:00
Case 11	4.4 cal ka BP	Typhoon 0509		
Case 12	4.4 cal ka BP	Typhoon 9711	1997-07-21 14:00:00	1997-08-21 08:00:00

Table 3
The mean spring high waters (MSHW) and highest water levels (HWL) during different typhoon scenarios in each sub-basins from 7.6 to 4.5 cal ka BP.

Sub-basins			7.6 cal ka BP	6.4 cal ka BP	4.5 cal ka BP
Yangtze Estuary	MSHW	Mouth	1.6	1.6	1.8
	HWL during TP0509		2.0	1.8	2.0
	HWL during TP9711		2.0	1.8	2.0
	MSHW	Head	2.0	1.8	2.2
	HWL during TP0509		2.4	2.4	2.2
	HWL during TP9711		2.4	2.4	2.4
Hangzhou Bay	MSHW	Mouth	1.6	1.6	2.0
	HWL during TP0509		1.8	1.6	2.0
	HWL during TP9711		2.0	1.8	2.2
	MSHW	Head	1.4	1.6	2.2
	HWL during TP0509		2.2	2.4	3.2
	HWL during TP9711		2.4	2.4	3.2
Paleo-Taihu Estuary	MSHW	Mouth	1.4	1.6	infilled
	HWL during TP0509		2.4	2.4	infilled
	HWL during TP9711		2.2	2.2	infilled
	MSHW	Head	1.2	1.4	infilled
	HWL during TP0509		2.6	2.0	infilled
	HWL during TP9711		2.4	2.0	infilled
West Taihu Valley	MSHW		0.6	0.8	infilled
	HWL during TP0509		1.4	1.4	infilled
	HWL during TP9711		1.6	1.4	infilled
Yaojiang Valley	MSHW		1.4	1.2	1.0
	HWL during TP0509		1.4	1.2	1.4
	HWL during TP9711		1.8	1.8	1.6
Ningbo Bay	MSHW	Mouth	1.2	1.0	1.4
	HWL during TP0509		1.4	1.2	1.6
	HWL during TP9711		1.8	1.6	1.8
	MSHW	Head	1.6	1.4	1.2
	HWL during TP0509		1.8	1.4	1.4
	HWL during TP9711		2.0	2.0	1.6

Yangtze Estuary, Yaojiang Valley and Ningbo Bay at three stages. Furthermore, the storm surge at three stages was all generally higher in the scenario of TP9711 than TP0509 in the Yaojiang Valley and Ningbo Bay, southeast coast of Hangzhou Bay (Table 3; Fig. 7). In the Yangtze Estuary, it was also slightly higher in the scenario of TP9711. The storm surge was similar in both typhoon scenarios in Hangzhou Bay, but slightly higher in the scenario of TP0509 in the paleo-Taihu Estuary.

The storm inundation mainly occurred along the coastlines and its spatial extent was larger in scenario TP9711 than TP0509 at all three stages. All sites in Fig. 2 were inundated at 7.6 and 6.4 cal ka BP in both typhoon scenarios (Figs. 8, 9). At 4.5 cal ka BP, sites 4 (DTX4) and 5 (WJB) were free from the flooding in both scenarios because of the seaward advance of the coastline, although the inundation extent was larger than earlier stages. Such simulation results agreed with the sedimentary records (Fig. 2). In addition, little inundation occurred in the Yaojiang Valley and Ningbo Plain in scenario TP0509, and the Neolithic Yushan and TLS sites (No. 1 and 2, respectively in Figs. 2, 10) was only inundated in scenario TP9711 at 4.5 cal ka BP.

4.4. Inundations in the scenario of sea-level rise at 4.4 cal ka BP

In the scenario of relative sea-level rise for 0.95 m at 4.4 cal ka BP, the submerged area of highest astronomical tide (Fig. 11) was significantly larger than that in scenario TC0509 (Fig. 10A) and similar to that in the scenario TC9711 (Fig. 10B) at 4.5 cal ka BP. The coastal lowlands along the Yangtze Estuary and Hangzhou Bay, which was only submerged during extreme storm events at 4.5 cal ka BP, was flooded regularly every month in the scenario of sea-level rise at 4.4 cal ka BP. Sea-level rise also aggravated the saltwater intrusion in the Ningbo Plain and Yaojiang Valley, and the flooding reached deeper inland. All sites in Fig. 2 except sites 4 and 5 were inundated by the sea flooding.

Sea-level rise also indirectly increased the intensity of storm surge in scenarios of extreme events. In the scenario TC0509 (Fig. 11A), the storm surge coupled with sea-level rise significantly flooded the larger area of coastal plain along the Yangtze Estuary and Hangzhou Bay including almost half of the Taihu Plain. The TC9711 caused a more serious flooding compared to TC0509 (Fig. 11B). However, the location of DTX4 (site 4) was always free from the sea flooding. On the south bank of Hangzhou Bay, the saltwater during the two storm events approached the foothills of Siming Mountain and submerged most part of the Yaojiang Valley and Ningbo Plain (Fig. 11B).

5. Discussions

5.1. Mechanism of the temporal changes in tidal levels along the coast of Hangzhou Bay

The simulation results demonstrated significant tidal amplification in Hangzhou Bay from 6.4 to 4.5 cal ka BP (Figs. 6B–C, 7; Table 3), which we suggest induced by the infilling of the paleo-Taihu Estuary and the progradation of the south Yangtze Delta plain. Previous studies showed that the tidal wave propagation was impacted by both the geometric shape and the bottom friction of the estuary (Savenije et al., 2008). Without loss of friction, the narrowing of the estuary width will concentrate the tidal wave energy, which amplifies the tidal range; when the estuary shape remains unchanged, bottom friction counters part of the tidal energy, depending on water depth and bed roughness, and tidal range decreases (Savenije et al., 2008). The infilling of the paleo-Taihu Estuary and progradation of delta plain after 6.4 cal ka BP resulted in the narrowing widths at the head of Hangzhou Bay at 4.5 cal ka BP, while the water depth in the bay changed little from 6.4 to 4.5 cal ka BP (Fig. 3). Thus, landward narrowing of the bay occurred without the increase in bottom friction at 4.5 cal ka BP, which led to an overall increase in the tidal levels in the bay and a significant amplification at its head (Fig. 6C).

Of note, the Yaojiang Valley and Ningbo Bay on the southeast coast of the bay were mostly infilled and turned into the coastal plain at 4.5 cal ka BP (Fig. 3F), which would increase the bottom friction largely and reduce the tidal range there (Fig. 6C). Similar tidal weakening induced by infilling and decrease in the length of the bay during the

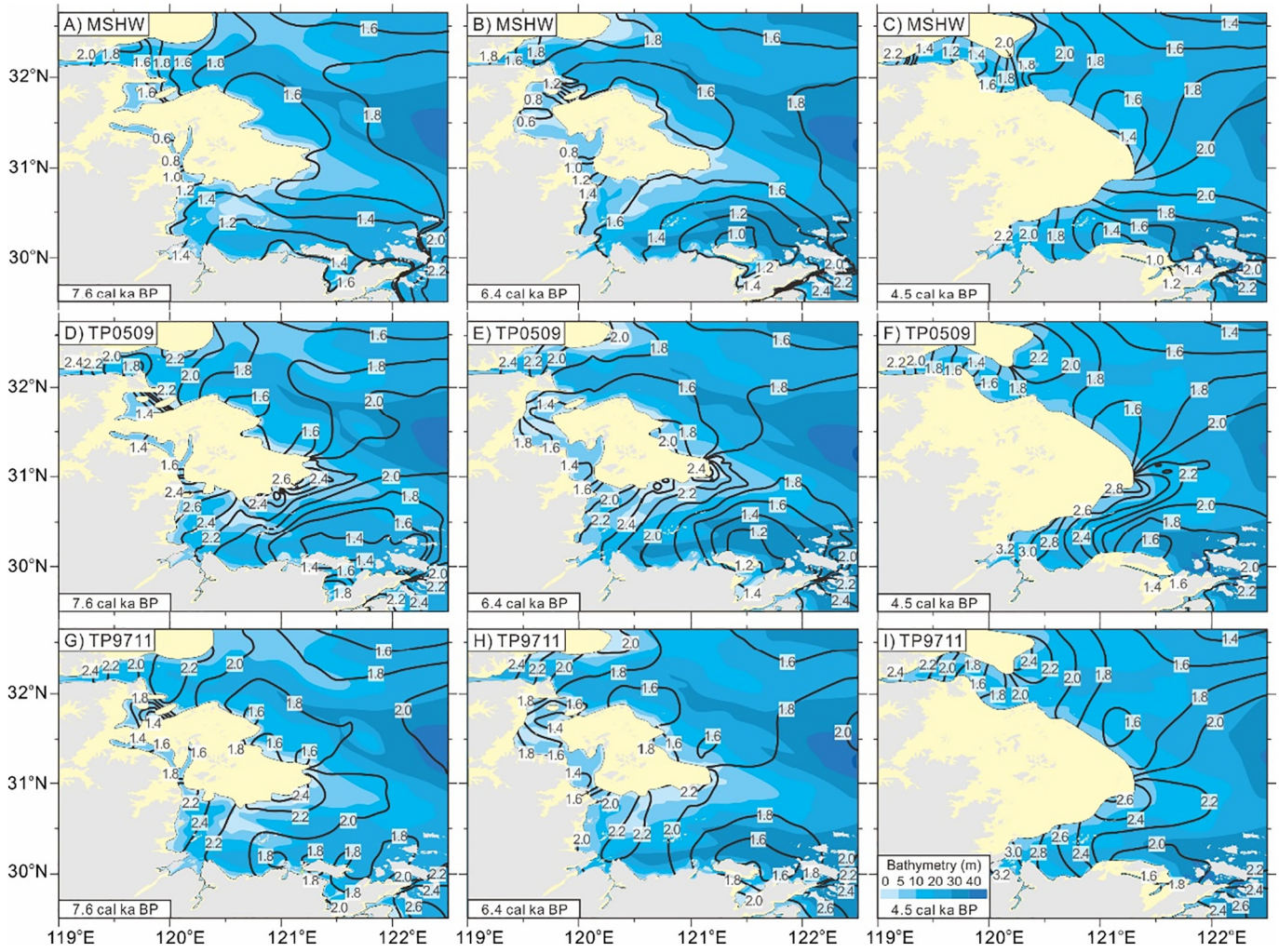

Fig. 6. Spatial distributions of MSHW at 7.6 (A), 6.4 (B), and 4.5 cal ka BP (C), peak water elevations at 7.6 (D), 6.4 (E), and 4.5 cal ka BP (F) in the scenario TC0509 and peak water elevations at 7.6 (G), 6.4 (H), and 4.5 cal ka BP (I) in the scenario TC9711. Numbers in A–C denote the highest tide levels in the one-month tide simulation, representing the mean spring high water (MSHW). Numbers in D–I denote the highest water levels in the storm-tide simulation under two typhoon scenarios.

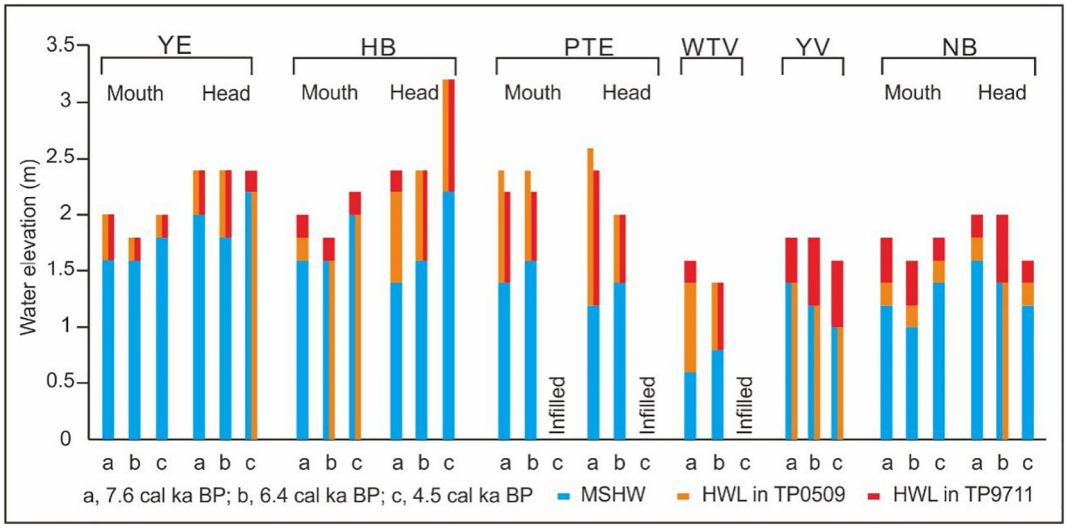

Fig. 7. Temporal changes in the simulated water elevations including the MSHW in fair weather and HWL in the two typhoon scenarios. Abbreviation: YE, Yangtze Estuary; HB, Hangzhou Bay; PTE, paleo-Taihu Estuary; WTV, west Taihu Valley; YV, Yaojiang Valley; NB, Ningbo Bay.

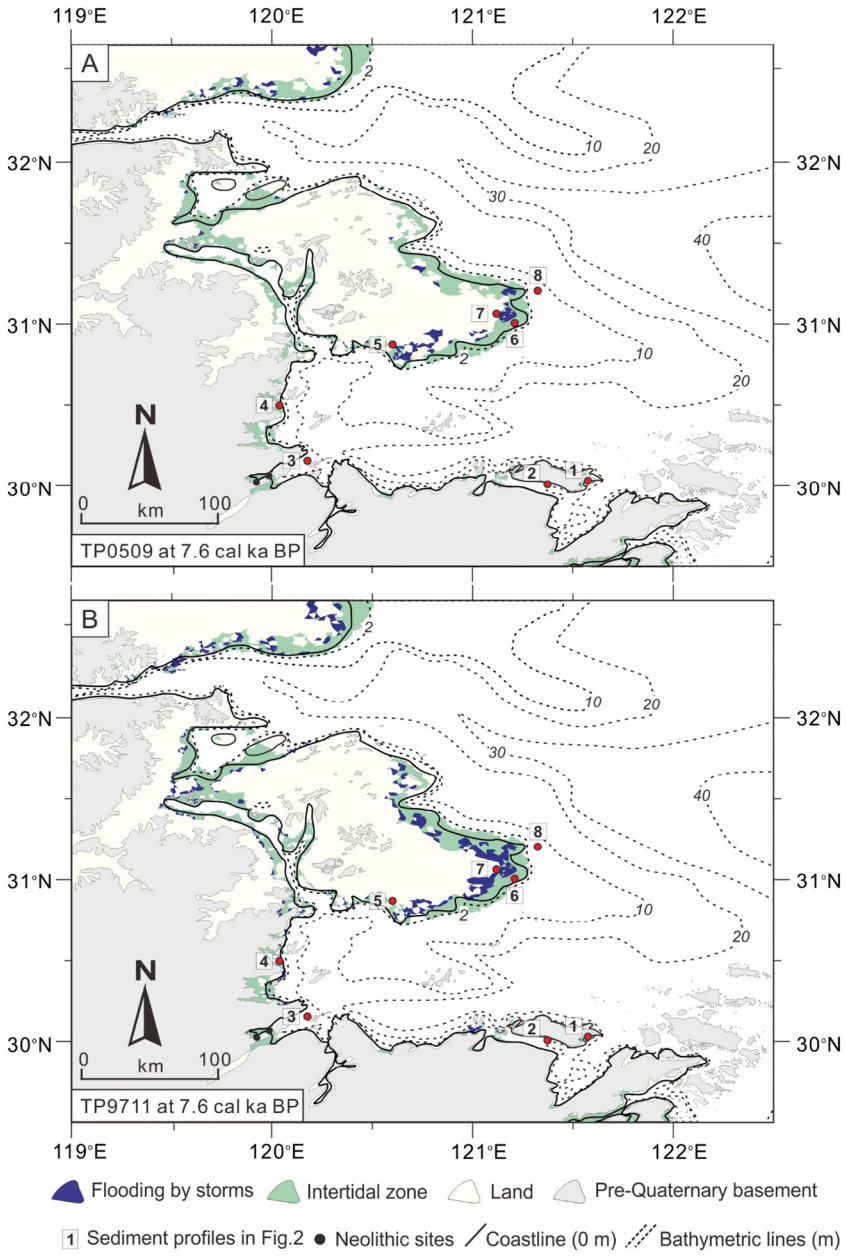

Fig. 8. Distributions of intertidal zone at 7.6 cal ka BP and flooding areas by storms at flooding peak time in the scenarios TC0509 (A) and TC9711 (B).

Holocene has also been reported in Tokyo Bay (Uehara and Saito, 2019).

5.2. The mechanism of marine flooding and relative sea-level rise at 4.5–4.4 cal ka BP

Based on above simulated results of the water elevations and inundation areas during the spring tides, we suggest that both the tidal amplification and relative sea-level rise should be considered for the formation mechanism of the transgressive layers preserved at the Neolithic sites in the south Yangtze coastal plain in the period from 7.6 to 4.5 cal ka BP. In addition, tropical cyclone was still an important mechanism for short-term marine invasion in this region.

Obvious rise in both global and regional sea levels occurred at 7.6 cal ka BP (Bird et al., 2007; Wang et al., 2012), which would have formed marine sediments at the coastal sites at that time (Figs. 2, 8). At 6.4 cal ka BP, the west Taihu Valley, paleo-Taihu Estuary, Yaojiang Valley and Ningbo Bay were all submerged by sea water due to the sea-level rise (Figs. 3B, 9; Chen et al., 2018). The coastal sites were easily inundated during the storm events (Fig. 9), which could explain the marine and brackish diatom species, marine species of dinoflagellate cysts found in the transgressive layers there (Fig. 2; Qin et al., 2011; Zheng et al., 2012; Chen et al., 2018). By contrast, as infilling and terrestrialization occurred in the paleo-Taihu Estuary, Yaojiang Valley and Ningbo Bay at 4.5 cal ka BP, some of the sites (e.g., sites 1, 2, 4, 5, 6, 7; Fig. 10) were free from the spring tides in the fair weather and could only be inundated in scenarios of extreme events (Fig. 10B) or sea-level rise (Fig. 11). Therefore, here we mainly focus on the mechanism of marine flooding at 4.5 cal ka BP.

The decline in tidal amplitude in the southeast coastal plain of Hangzhou Bay from 7.6 to 4.5 cal ka BP (Table 3; Fig. 7) ruled out the factor of tidal amplification for the marine flooding in the Yaojiang Valley and Ningbo Plain at 4.5 cal ka BP (Fig. 2). The simulation results of scenario TP9711 (Fig. 10B) agreed well with the storm deposits covering the Liangzhu cultural layer reported at the Yushan site (Fig. 2; Wang et al., 2018a). However, storm events could only induce short-

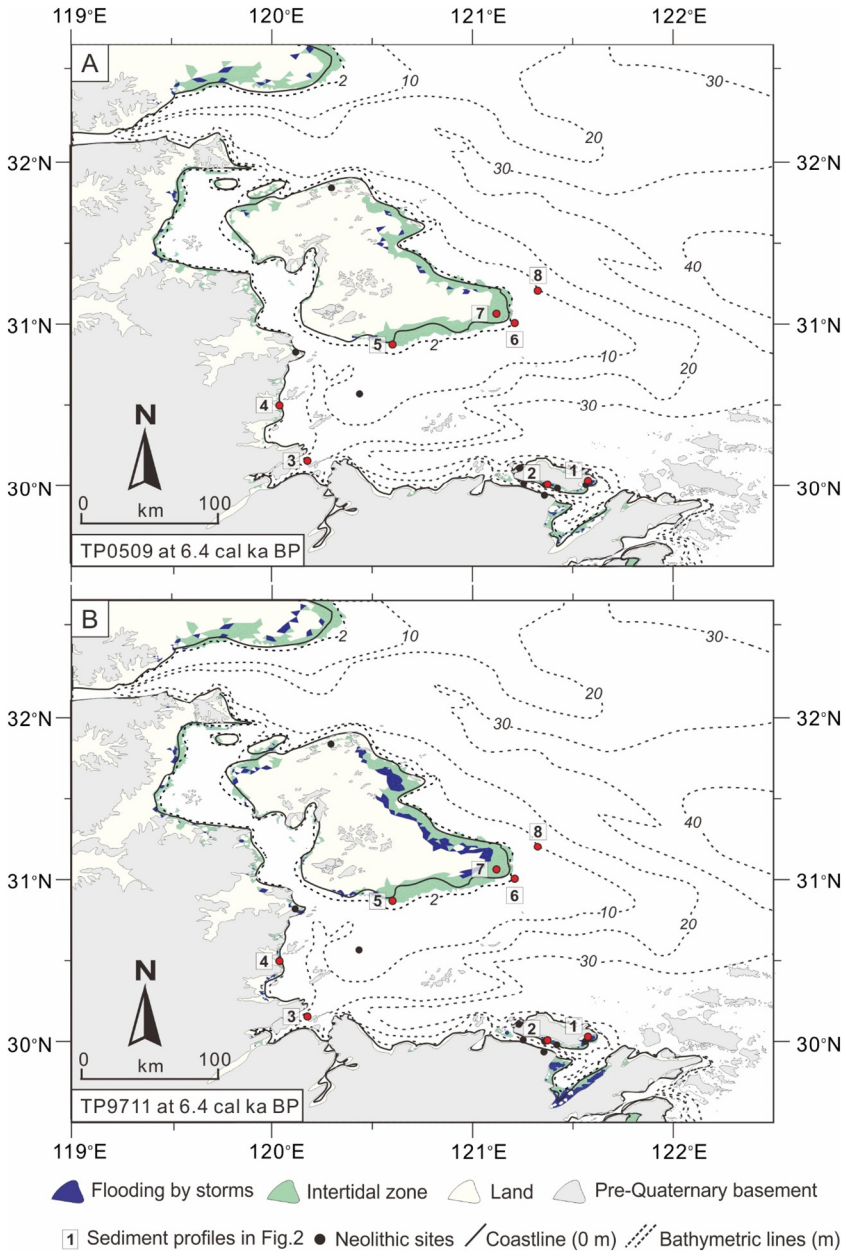

Fig. 9. Distributions of intertidal zone at 6.4 cal ka BP and flooding areas by storms at flooding peak time in the scenarios TC0509 (A) and TC9711 (B).

term inundation, whilst the marine flooding following the storm event occurred continually for ca. 1000 yrs. at the Yushan site and long period at TLS site (Fig. 2; Zheng et al., 2012). Therefore, we speculate that this marine transgression in the Yaojiang Valley and Ningbo Plain could have been caused by a local relative sea-level rise. Such speculation was evidenced by our simulation in the 4.4 cal ka BP scenario (Fig. 11), in which a relative sea-level rise of 0.95 m was added. In our simulation, the coastal lowland in the Ningbo Plain, which was only submerged during extreme storm events at 4.5 cal ka BP (Fig. 10B), was flooded regularly every month in the scenario of sea-level rise at 4.4 cal ka BP. The Neolithic sites TLS and Yushan in the Yaojiang Valley and Ningbo Plain were inundated by spring tides in the 4.4 cal ka BP scenario (Fig. 11), which agreed with the inference of upper tidal flat environment at Yushan site (Wang et al., 2018a) and the termination of rice cultivation at TLS site at that time (Zheng et al., 2012).

5.3. The extreme storm events at 4.5 cal ka BP

Our simulation suggested that the Yushan site can only be submerged in the storm scenario of TC9711, not the TC0509 at 4.5 cal ka BP (Fig. 10). Thus, the previously reported Yushan storm (Wang et al., 2018a) was most likely an extreme event, larger than the typical typhoons that landed on Hangzhou Bay and the east China coast frequently, or it was a typhoon that made landfall directly in the study area. In addition to the direct evidence of storm deposits at Neolithic Yushan and GFL sites (Wang et al., 2018a; Tang et al., 2019), reports of buried trees in the artefacts-absent layers covering the Liangzhu cultural layers at many Neolithic sites provided evidences of the occurrence of extreme events at the late stage of Neolithic culture (Cheng and Song, 1999). There were also a few radiocarbon ages at ~4000–4300 BP (uncalibrated) obtained from the storm-generated chenier ridges on the Yangtze coast (Yan et al., 1989). We thus speculate that a period of frequent extreme events occurred simultaneously with the abrupt sea-level rise at 4.5–4.4 cal ka BP. Extreme typhoon events around

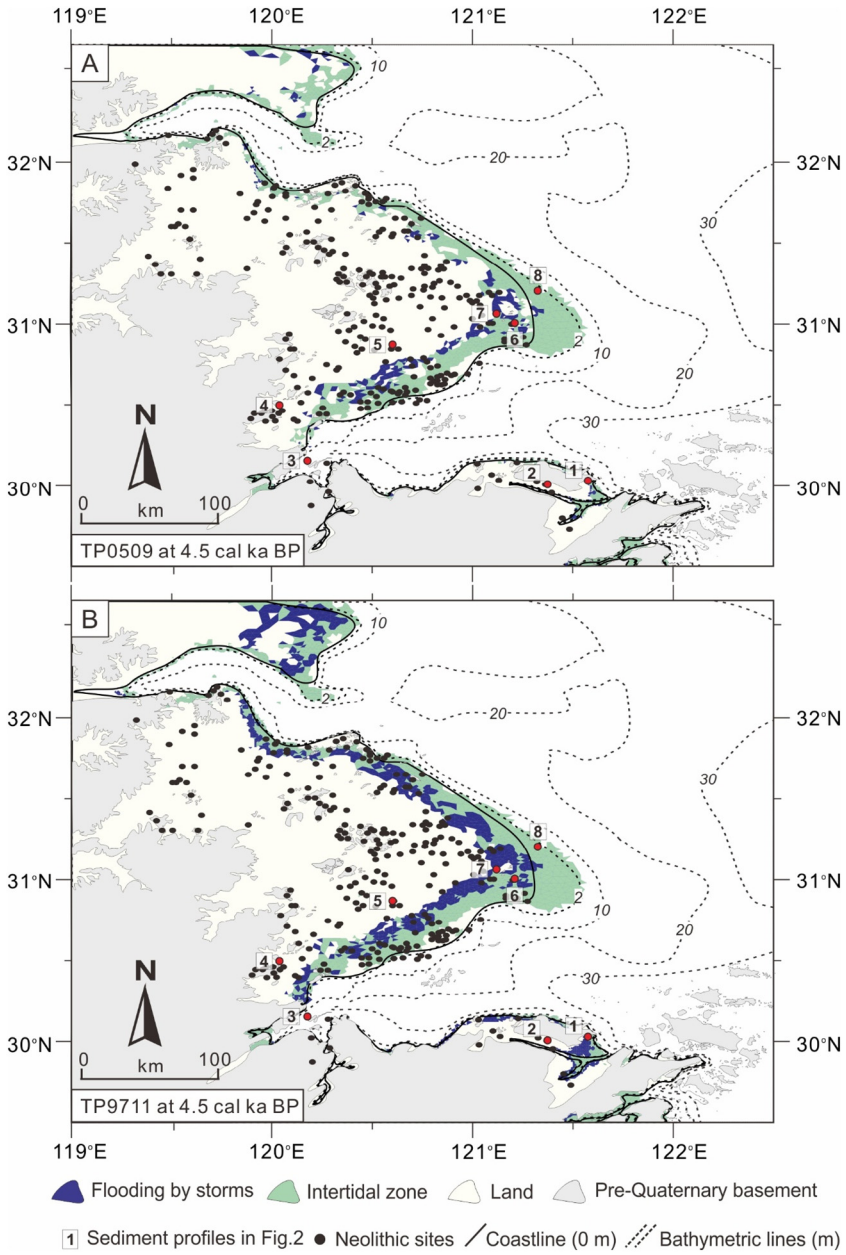

Fig. 10. Distributions of intertidal zone at 4.5 cal ka BP and flooding areas by storms at flooding peak time in the scenarios TC0509 (A) and TC9711 (B).

4.5 cal ka BP have also been recognized from the sedimentary records in the lagoon and coastal lakes in Korean Peninsula and Japan (Woodruff et al., 2009; Katsuki et al., 2017). We suggest that further research is necessary to work on the linkage between the abrupt sea-level rise and frequent extreme typhoon events at that time.

However, storm deposits have been less reported from the north bank of Hangzhou Bay, except the records at chenier ridges on the coastal line (e.g. MQ site in Fig. 2; Yan et al., 1989). The chenier ridges possibly played important role on protecting the inland from marine inundation during the extreme events. But there are still many limitations in studying the storm deposits in this area. One reason is that sedimentary profiles with substantial age control data are still very limited from the area; and erosion has occurred and led to the landward retreat of shoreline on the north bank of the bay in the late Holocene (Zong et al., 2012). Another difficulty is that storm deposits in the study area are always characterized by fine-grained sediments, which hinders their recognition (Xu, 1997); so storm deposits could exist but have not been recognized. Further work on recognizing the storm deposits is necessary in the study area.

5.4. Flood risk and the Neolithic settlements

Before the infilling of the paleo-Taihu Estuary, at 7.6 and 6.4 cal ka BP in our simulations, the Taihu Plain was susceptible by marine flooding both in spring and storm tides (Figs. 6, 8, 9). Such high flood risk may explain why the early Neolithic settlements appeared first in more upland areas such as the Kuahuqiao site (Zong et al., 2007; Innes et al., 2009). The existence of the west Taihu Valley and development of a paleo-Taihu Estuary further increased the flood risk in the west part of the Taihu Plain, while the east and north parts were less susceptible to inundation. Previous archaeological studies reported a reduction in the human settlements around the paleo-Taihu Estuary and an increase in the east and north part of the Taihu Plain during the middle to late Majiabang Culture (6500–6000 cal a BP) (Wu, 1988; Zheng, 2007). We speculate that the Neolithic people living in the area were forced to migrate to the east and north parts of the Taihu Plain to avoid marine

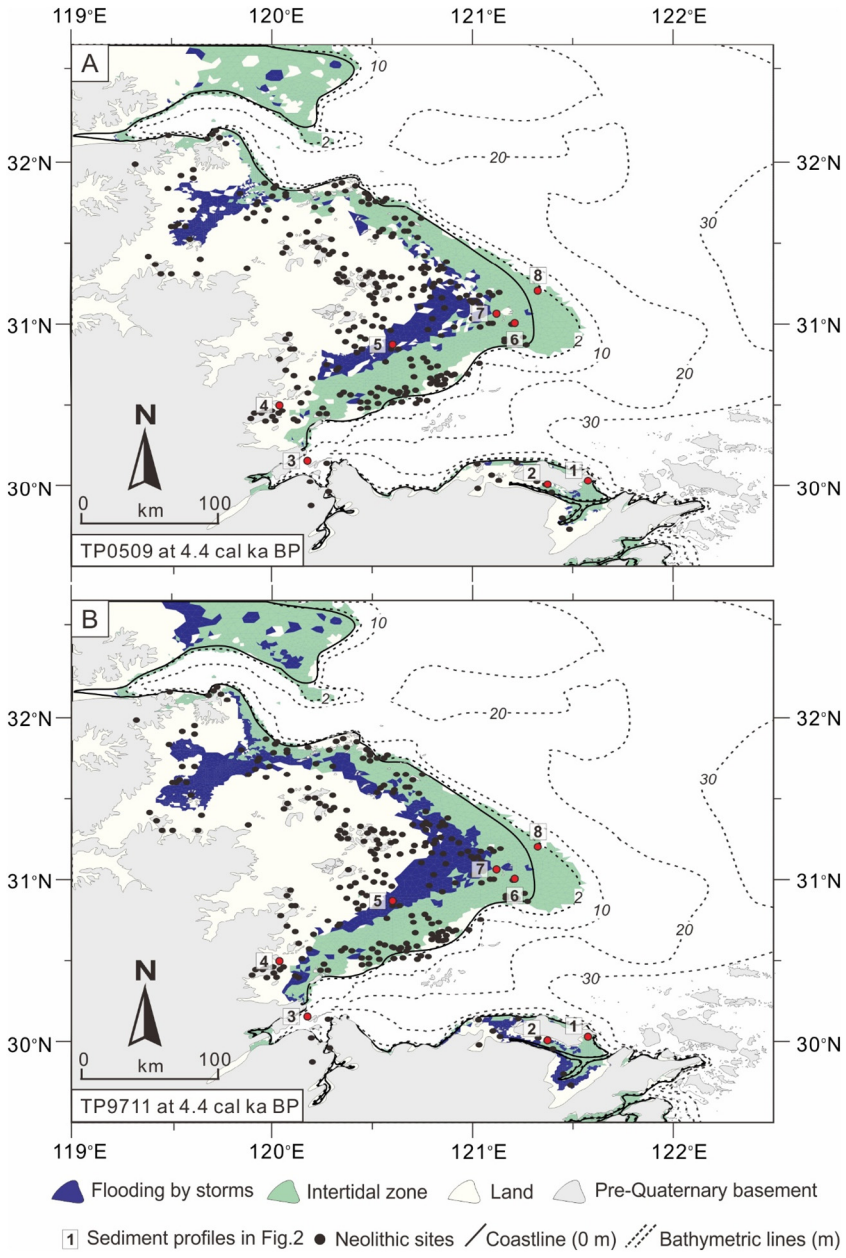

Fig. 11. Distributions of intertidal zone at 4.4 cal ka BP and flooding areas by storms at flooding peak time in the scenarios TC0509 (A) and TC9711 (B) under 0.95-m sea-level rise.

flooding in the middle and late stages of Majiabang Culture. Human settlements were also restricted in the east and north parts of the Taihu Plain in the early and middle stages of the Songze Culture (5800–5500 cal a BP) (Wu, 1988), potentially for the same reason. By contrast, the Hemudu Culture (7200–5300 cal a BP) lasted for about 2000 years in Yaojiang Valley and Ningbo Bay and the human settlements increased rapidly after ca. 6.5 cal ka BP there (Jiang et al., 1999). We suggest that the Neolithic people preferred this area at that time, because the coastal plain here was sheltered by uplands with much lower spring and storm tidal levels (Fig. 6D–F).

After the infilling of the paleo-Taihu Estuary at ca. 5.6 cal ka BP, the freshwater and land resources increased abruptly in the Taihu Plain (Chen et al., 2018). Furthermore, the central and west Taihu Plain was safe from the marine flooding, even in the scenario of an extreme storm event (Fig. 10). We suggest that such an environment with large amount of freshwater and land sources was beneficial for the rapid development of the rice production, which contributed to the rapid expansion of the Liangzhu society in the Taihu Plain during 5.3–4.5 cal ka BP (Fig. 10; Zheng, 2007; Mo et al., 2011; Chen, 2014).

However, as discussed above, our simulation supported the previous speculation of an event of relative sea-level rise from 4.5 cal ka BP (Wang et al., 2018a). Together with the significant tidal amplification and storm surge in Hangzhou Bay (Figs. 6G–I), persistent flood risk of both inland and marine origin would have occurred in the study area at that time (Fig. 11). The capital city of the Liangzhu Culture was even close to the marine flooding in the scenarios of both sea-level rise and extreme events (Fig. 11). Such frequent inundation events would have been a particularly severe disaster for rice cultivation, potentially weakening the economic foundation of the Liangzhu society (Liu et al., 2017). We thus speculate that the increased risk of coastal flooding played an important role in the abrupt abandonment of the capital city and the termination of the Liangzhu Culture in the south Yangtze coastal plain at ca. 4.5–4.4 cal ka BP (Zhang et al., 2015b; Wang et al., 2018a).

6. Conclusions

This study reconstructed the paleo-topography of the south Yangtze coast at 7.6, 6.4 and 4.5 cal ka BP based on a large database of sediment cores, Neolithic site profiles and radiocarbon ages from these cores and profiles. The tidal regimes and storm-tides were further simulated using high-resolution CE-FVCOM to estimate the water elevations and inundation areas during the spring tide and storm tides of two typhoon scenarios at each of the targeted time periods. Several conclusions can be derived from our results as below.

1. The high tidal levels were reduced in the southeast coastal plain of Hangzhou Bay from 7.6 to 4.5 cal ka BP, because of the increased bottom friction and decreased length of Ningbo Bay induced by the infilling and shoaling bathymetry of the coastal zones, although an overall tidal amplification occurred in Hangzhou Bay owing to its narrowing in the head. Such decrease in tidal amplitude indicated that the long-lasting marine flooding in the Yaojiang Valley and Ningbo Plain after 4.5 cal ka BP was favorable to be induced by relative sea-level rise rather than the tidal amplification.
2. Simulation of storm-tides in different scenarios indicated that only extreme events similar or stronger than Typhoon 9711 could explain the storm deposits reported from the Ningbo Plain at 4.5 cal ka BP.
3. Marine flooding through the paleo-Taihu Estuary and west Taihu Valley likely limited the development of prehistoric societies in the Taihu Plain in the early stages of Neolithic culture, while the sheltered environment by uplands in the Yaojiang Valley-Ningbo Plain promoted the expansion of the Hemudu Culture there.
4. The risk of coastal flooding increased significantly in the Taihu Plain including in region close to the capital city of the Liangzhu Culture in the scenario of sea-level rise at 4.4 cal ka BP, which we infer was a major cause for the abandonment of the capital city and termination of Culture.

Declaration of competing interest

The authors declare that they have no known competing financial interests or personal relationships that could have appeared to influence the work reported in this paper.

Acknowledgements

This study was supported by the National Natural Science Foundation of China (Grant No. 41576042) and the Open Research Fund of State Key Laboratory of Estuarine and Coastal Research (Grant No. SKLEC-PGKF201902). The authors are indebted to Dr. Meng Xia and graduate students in the Department of Natural Sciences, University of Maryland Eastern Shore, who assisted in model settings and the language corrections. Authors are also grateful for three anonymous reviewers for their valuable comments.

Appendix A. Supplementary data

Supplementary data to this article can be found online at https://doi.org/10.1016/j.margeo.2020.106134.

References

Bird, M.I., Fifield, L.K., Teh, T.S., Chang, C.H., Shirlaw, N., Lambeck, K., 2007. An inflection in the rate of early mid-Holocene eustatic sea-level rise: a new sea-level curve from Singapore. Estuar. Coast. Shelf Sci. 71, 523–536.
Blaauw, M., 2010. Methods and code for 'classical' age-modelling of radiocarbon sequences. Quat. Geochronol. 5, 512–518.
Cai, W., Wang, G., Dewitte, B., Wu, L., Santoso, A., Takahashi, K., Yang, Y., Carreric, A., McPhaden, M.J., 2018. Increased variability of eastern Pacific El Nino under greenhouse warming. Nature 564, 201–206.
Chen, J., 2014. The paleo-environment of Liangzhu culture (in Chinese). Hangzhou Press.
Chen, J., Chen, Z., Li, C., 2007. Environmental analysis of Guangfulin site in Songjiang district, Shanghai. Archaeology (in Chinese) 7, 71–79.
Chen, C., Liu, H., Beardsley, R.C., 2003. An unstructured grid, finite-volume, three-dimensional, primitive equations ocean model: application to coastal ocean and estuaries. J. Atmos. Ocean. Technol. 20, 159–186.
Chen, T., Ryves, D.B., Wang, Z., Lewis, J.P., Yu, X., 2018. Mid- to late Holocene geomorphological and hydrological changes in the south Taihu area of the Yangtze delta plain, China. Palaeogeogr. Palaeoclimatol. Palaeoecol. 498, 127–142.
Cheng, P., Song, C., 1999. The contributing factors for the discontinuity of Liangzhu culture and its trend. Southeast Culture 4, 14–21 (in Chinese).
Zong, Y., Innes, J.B., Wang, Z., Chen, Z., 2011. Mid-Holocene coastal hydrology and salinity changes in the east Taihu area of the lower Yangtze wetlands, China. Quat. Res. 76, 69–82.
Zong, Y., Innes, J.B., Wang, Z., Chen, Z., 2012. Environmental change and Neolithic settlement movement in the lower Yangtze wetlands of China. The Holocene 22, 659–673.
ECCHE (Editorial Committee for Chinese Harbors and Embayments), 1992. Chinese Harbours and Embayments (Part V) China Ocean Press, Beijing (in Chinese).
Egbert, G.D., Erofeeva, S.Y., 2002. Efficient inverse modeling of barotropic ocean tides. Journal of Atmospheric & Oceanic Technology 19, 183–204.
Fujita, T., 1952. Pressure distribution within typhoon. Geophys. Mag. 23, 437–451.
Gao, S., Collins, M.B., 2014. Holocene sedimentary systems on continental shelves. Mar. Geol. 352, 268–294.
Ge, J., 2007. Numerical Forecasting and Visualization of Storm Surge. Ph.D. Dissertation. East China Normal University (in Chinese).
Ge, J., Ding, P., Chen, C., Hu, S., Fu, G., Wu, L., 2013. An integrated East China Sea-Changjiang Estuary model system with aim at resolving multi-scale regional-shelf-estuarine dynamics. Ocean Dyn. 63, 881–900.
Grinsted, A., Moore, J.C., Jevrejeva, S., 2013. Projected Atlantic hurricane surge threat from rising temperatures. Proc. Natl. Acad. Sci. 110, 5369–5373.
He, K., Lu, H., Zheng, Y., Zhang, J., Xu, D., Huan, X., Wang, J., Lei, S., 2018. Middle-Holocene sea-level fluctuations interrupted the developing Hemudu culture in the lower Yangtze River, China. Quat. Sci. Rev. 188, 90–103.
Hinkel, J., Lincke, D., Vafeidis, A.T., Perrette, M., Nicholls, R.J., Tol, R.S., Marzeion, B., Fettweis, X., Ionescu, C., Levermann, A., 2014. Coastal flood damage and adaptation costs under 21st century sea-level rise. Proc. Natl. Acad. Sci. 111, 3292–3297.
Hong, X.Q., 1991. Origin and evolution of the Taihu lake. Mar. Geol. Quat. Geol. 4, 87–99 (in Chinese).
Hori, K., Saito, Y., Zhao, Q., Cheng, X., Wang, P., Sato, Y., Li, C., 2001. Sedimentary facies and Holocene progradation rates of the Changjiang (Yangtze) delta, China. Geomorphology 41, 233–248.
Innes, J.B., Zong, Y., Chen, Z., Chen, C., Wang, Z., Wang, H., 2009. Environmental history, palaeoecology and human activity at the early Neolithic forager/cultivator site at Kuahuqiao, Hangzhou, eastern China. Quat. Sci. Rev. 28, 2277–2294.
Jackson, L.P., Grinsted, A., Jevrejeva, S., 2018. 21st century sea-level rise in line with the Paris Accord. Earth's Future 6, 213–229.
Jiang, D., Wang, X., Hao, W., 1999. Mid-Holocene paleoclimatic-paleoenvironmental changes in Zhejiang Province and Hemudu ancients. Universitatis Pekinensis (Acta Scientiarum Naturalium) 35 (2), 248–253 (in Chinese).
Katsuki, K., Yang, D.-Y., Lim, J., Lee, J.-Y., Asahi, H., Han, M., 2017. Multi-centennial-scale changes in East Asian typhoon frequency during the mid-Holocene. Palaeogeogr. Palaeoclimatol. Palaeoecol. 476, 140–146.
Kopp, R.E., DeConto, R.M., Bader, D.A., Hay, C.C., Horton, R.M., Kulp, S., Oppenheimer, M., Pollard, D., Strauss, B.H., 2017. Evolving understanding of Antarctic ice-sheet physics and ambiguity in probabilistic sea-level projections. Earth's Future 5, 1217–1233.
Li, Y., Wu, J., Hou, S., Shi, C., Mo, D., Liu, B., Zhou, L., 2010. Palaeoecological records of environmental change and cultural development from the Liangzhu and Qujialing archaeological sites in the middle and lower reaches of the Yangtze River. Quat. Int. 227, 29–37.
Liu, B., Wang, N., Chen, M., Wu, X., Mo, D., Liu, J., Xu, S., Zhuang, Y., 2017. Earliest hydraulic enterprise in China, 5,100 years ago. Proc. Natl. Acad. Sci. 114, 13637.
Liu, C., Walker, H.J., 1989. Sedimentary characteristics of cheniers and the formation of the Chenier Plains of East China. J. Coast. Res. 5, 353–368.
Long, T., Qin, J., Atahan, P., Mooney, S., Taylor, D., 2014. Rising waters: new geoarchaeological evidence of inundation and early agriculture from former settlement sites on the southern Yangtze Delta, China. The Holocene 24, 546–558.
Milliman, J.D., Syvitski, J.P.M., 1992. Geomorphic/tectonic control of sediment discharge to the ocean: the importance of small mountainous rivers. The Journal of Geology 100, 525–544.
Milliman, J.D., Huang-ting, S., Zuo-sheng, Y.H., Mead, R., 1985. Transport and deposition of river sediment in the Changjiang estuary and adjacent continental shelf. Continental Shelf Research 4, 37–45.
Miyazaki, M., Ueno, T., Unoki, S., 1961. Theoretical investigations of typhoon surges along the Japanese coast. Oceanographical Magazine 13, 51–75.
Mo, D., Zhao, Z., Xu, J., Li, M., 2011. Holocene environmental changes and the evolution of the Neolithic cultures in China. In: Martini, I.P., Chesworth, W. (Eds.), Landscapes and Societies: Selected Cases. Springer Netherlands, Dordrecht, pp. 299–319.
Nauels, A., Meinshausen, M., Mengel, M., Lorbacher, K., Wigley, T.M.L., 2017. Synthesizing long-term sea level rise projections–the MAGICC sea level model v2.0. Geosci. Model Dev. 10, 2495–2524.
Neumann, B., Vafeidis, A.T., Zimmermann, J., Nicholls, R.J., 2015. Future coastal population growth and exposure to sea-level rise and coastal flooding–a global assessment. PLoS One 10, e0118571.
Qin, J., Taylor, D., Atahan, P., Zhang, X., Wu, G., Dodson, J., Zheng, H., Itzstein-Davey, F., 2011. Neolithic agriculture, freshwater resources and rapid environmental changes on the lower Yangtze, China. Quat. Res. 75, 55–65.

Ren, Z.Y., Wang, B.L., Fan, T.T., Liu, H., 2013. Numerical analysis of impacts of 2011 Japan Tohoku tsunami on China Coast. J. Hydrodyn. Ser. B 25, 580–590.
Rogelj, J., Meinshausen, M., Knutti, R., 2012. Global warming under old and new scenarios using IPCC climate sensitivity range estimates. Nat. Clim. Chang. 2, 248–253.
Savenije, H.H.G., Toffolon, M., Haas, J., Veling, E.J.M., 2008. Analytical description of tidal dynamics in convergent estuaries. J. Geophys. Res. 113.
Song, B., Li, Z., Saito, Y., Okuno, J., Li, Z., Lu, A., Hua, D., Li, J., Li, Y., Nakashima, R., 2013. Initiation of the Changjiang (Yangtze) delta and its response to the mid-Holocene sea level change. Palaeogeogr. Palaeoclimatol. Palaeoecol. 388, 81–97.
Song, J., Zhou, L., Chen, J., 2002. The excavated report on the Neolithic site Guangfulin, Songjiang, Shanghai during 1999-2000. Archaeology 10, 31–48 (in Chinese).
Stuiver, M., Reimer, P.J., Reimer, R.W., 2018. CALIB: radiocarbon calibration. http://calib.qub.ac.uk/calib/ (September 2018).
Tang, L., Shu, J., Chen, J., Wang, Z., 2019. Mid- to late Holocene vegetation change recorded at a Neolithic site in the Yangtze coastal plain, East China. Quaternary International 519, 122–130.
Tessler, Z.D., Vörösmarty, C.J., Grossberg, M., Gladkova, I., Aizenman, H., Syvitski, J.P.M., Foufoula-Georgiou, E., 2015. Profiling risk and sustainability in coastal deltas of the world. Science 349, 638.
Uehara, K., Saito, Y., 2003. Late Quaternary evolution of the Yellow/East China Sea tidal regime and its impacts on sediments dispersal and seafloor morphology. Sediment. Geol. 162, 25–38.
Uehara, K., Saito, Y., 2019. Tidal amplitude decreases in response to estuarine shrinkage: Tokyo Bay during the Holocene. Estuar. Coast. Shelf Sci. 225, 106225.
Uehara, K., Saito, Y., Hori, K., 2002. Paleotidal regime in the Changjiang (Yangtze) Estuary, the East China Sea, and the Yellow Sea at 6 ka and 10 ka estimated from a numerical model. Mar. Geol. 183, 179–192.
Wang, J., Lu, M., Ding, J., 2010. Analysis of temporal and spatial distribution characteristics of typhoon storm surges in coastal areas of Zhejiang province. Marine forecasts 27 (3), 16–22 (in Chinese).
Wang, Z., Zhuang, C., Saito, Y., Chen, J., Zhan, Q., Wang, X., 2012. Early mid-Holocene sea-level change and coastal environmental response on the southern Yangtze delta plain, China: implications for the rise of Neolithic culture. Quat. Sci. Rev. 35, 51–62.
Wang, Z., Zhan, Q., Long, H., Saito, Y., Gao, X., Wu, X., Li, L.I.N., Zhao, Y., 2013. Early to mid-Holocene rapid sea-level rise and coastal response on the southern Yangtze delta plain, China. J. Quat. Sci. 28, 659–672.
Wang, Z., Ryves, D.B., Lei, S., Nian, X., Lv, Y., Tang, L., Wang, L., Wang, J., Chen, J., 2018a. Middle Holocene marine flooding and human response in the south Yangtze coastal plain, East China. Quat. Sci. Rev. 187, 80–93.
Wang, Z., Saito, Y., Zhan, Q., Nian, X., Pan, D., Wang, L., Chen, T., Xie, J., Li, X., Jiang, X., 2018b. Three-dimensional evolution of the Yangtze River mouth, China during the Holocene: impacts of sea level, climate and human activity. Earth Sci. Rev. 185, 938–955.
Winterwerp, J.C., Wang, Z.B., van Braeckel, A., van Holland, G., Kösters, F., 2013. Man-induced regime shifts in small estuaries II: a comparison of rivers. Ocean Dyn. 63, 1293–1306.
Wong, T.E., Bakker, A.M.R., Keller, K., 2017. Impacts of Antarctic fast dynamics on sea-level projections and coastal flood defense. Clim. Chang. 144, 347–364.
Woodruff, J.D., Donnelly, J.P., Okusu, A., 2009. Exploring typhoon variability over the mid-to-late Holocene: evidence of extreme coastal flooding from Kamikoshiki, Japan. Quat. Sci. Rev. 28, 1774–1785.
Woodruff, J.D., Irish, J.L., Camargo, S.J., 2013. Coastal flooding by tropical cyclones and sea-level rise. Nature 504, 44–52.
Wu, J.M., 1988. The distribution and environmental changes of the prehistoric sites in Yangtze River delta. Southeast Culture 6, 16–36 (in Chinese).
Xie, D., Wang, Z., Gao, S., De Vriend, H.J., 2009. Modeling the tidal channel morphodynamics in a macro-tidal embayment, Hangzhou Bay. China. Continental Shelf Research 29, 1757–1767.
Xu, J., Liu, S., Jin, J., Mao, X., 2007. Characteristics of Tide level variation at upper reaches of Huangpu river during influence of Typhoon “Maisha” and analysis calculation. Urban Roads, Bridges & Flood Control 4, 14–19 (in Chinese).
Xu, S.Y., 1997. Storm Deposits in the Yangtze Delta. Science Press (in Chinese).
Yan, Q., Xu, S., Shao, X., 1989. Holocene cheniers in the Yangtze Delta, China. Mar. Geol. 90 (4), 337–343.
Ye, L., 1999. The forecast of storm surge disaster induced by Typhoon 9711. Marine Forecasts 16 (1), 67–70 (in Chinese).
Ying, M., Zhang, W., Yu, H., Lu, X., Feng, J., 2014. An overview of the China Meteorological Administration tropical cyclone database. J. Atmos. Ocean. Technol. 31, 287–301.
Yoneda, M., Uno, H., Shibata, Y., Suzuki, R., Kumamoto, Y., Yoshida, K., Sasaki, T., Suzuki, A., Kawahata, H., 2007. Radiocarbon marine reservoir ages in the western Pacific estimated by pre-bomb molluscan shells. Nucl. Instrum. Methods Phys. Res., Sect. B 259, 432–437.
Yu, S., Zhu, C., Shi, W., 1998. Middle and Late Holocene environmental changes of Maqiao, Shanghai. Acta Oceanol. Sin. 20 (1), 58–64 (in Chinese).
Zhang, Y., Xue, Y.Q., Wu, J.C., Yu, J., Wei, Z.X., Li, Q.F., 2008. Land subsidence and earth fissures due to groundwater withdrawal in the Southern Yangtze Delta, China. Environ. Geol. 55, 751–762.
Zhang, X., Ye, Y., Fang, X., 2012. Reconstruction of typhoons in the Yangtze River Delta during 1644-1949AD based on historical chorographies. J. Geogr. Sci. 22, 810–824.
Zhang, X., Dalrymple, R.W., Yang, S.Y., Lin, C.M., Wang, P., 2015a. Provenance of Holocene sediments in the outer part of the Paleo-Qiantang River estuary, China. Mar. Geol. 366, 1–15.
Zhang, X., Huang, D., Deng, H., Snape, C., Meredith, W., Zhao, Y., Du, Y., Chen, X., Sun, Y., 2015b. Radiocarbon dating of charcoal from the Bianjiashan site in Hangzhou: new evidence for the lower age limit of the Liangzhu Culture. Quat. Geochronol. 30, 9–17.
Zhao, C., Ge, J., Ding, P., 2014. impact of sea level rise on storm surges around the Changjiang Estuary. J. Coast. Res. 68, 27–34.
Zheng, J.M., 2007. The different development ways of the prehistoric cultures in the region of the Lower Changjiang River, China. Ph.D. dissertation, Fudan University (in Chinese).
Zheng, L., Yu, X., 2013. Interaction between storm surge and astronomical tide in Hangzhou Bay. Journal of Basic Science and Engineering 21 (1), 107–115 (in Chinese).
Zheng, Y., Sun, G., Chen, X., 2012. Response of rice cultivation to fluctuating sea level during the Mid-Holocene. Chin. Sci. Bull. 57, 370–378.
Zheng, Y., Sun, G., Qin, L., Li, C., Wu, X., Chen, X., 2009. Rice fields and modes of rice cultivation between 5000 and 2500 BC in east China. J. Archaeol. Sci. 36, 2609–2616.
Zong, Y., Chen, Z., Innes, J.B., Chen, C., Wang, Z., Wang, H., 2007. Fire and flood management of coastal swamp enabled first rice paddy cultivation in east China. Nature 449, 459–462.